# Potential of surface modified exosomes for extended intravitreal drug delivery

by

Derek Chen

A thesis

presented to the University of Waterloo

in fulfilment of the

thesis requirement for the degree of

Master of Science

in

Pharmacy

Waterloo, Ontario, Canada, 2021

## Author’s Declaration

This thesis consists of material all of which I authored or co-authored: see Statement of Contributions included in the thesis. This is a true copy of the thesis, including any required final revisions, as accepted by my examiners.

I understand that my thesis may be made electronically available to the public.

# Statement of Contributions

Derek Chen was the sole author of Chapters 2, 3, and 4 which were written under the supervision of Dr. Emmanuel Ho and were not written for publication.

This thesis consists in part of one manuscript written for publication. Exceptions to sole authorship of material are as follows:

Research presented in Section 1.6.1 and 1.6.2:

This review was conducted at the University of Waterloo by Jin Wang and Derek Chen under the supervision of Dr. Emmanuel Ho. Jin Wang and Derek Chen prepared the review with consultation from Dr. Emmanuel Ho who contributed to manuscript drafting and editing. Derek Chen contributed to figure preparation (Figure 2), manuscript drafting of the content presented in Section 1.6.1 – 1.6.2, and contributed to editing of the whole manuscript.

Citation:

Wang, J., Chen, D. & Ho, E. A. Challenges in the development and establishment of exosome-based drug delivery systems. *J Control Release* **329**, 894–906 (2020).

# Abstract

Diabetic retinopathy is a serious condition affecting retinal cells that can lead to blindness. Intravitreal injection is the only feasible method of drug delivery to the retina. However, intravitreal injections are only suitable for drugs with large therapeutic indices and long half-lives (the anti-VEGF agents). Drugs with less favourable properties would require multiple injections a week and are thus unfeasible to use. Still, the success of a monthly injection treatment plan of anti-VEGF agents is limited by compliance. There is a need to improve intravitreal drug delivery systems to reduce injection frequency and allow for delivery of molecules with unfavourable pharmacokinetics, such as small molecule drugs. Nanotechnology is a tool that can be used in drug delivery to improve properties such as drug solubility and stability. Exosomes are cell-derived nanoparticles which have recently shown promise as drug delivery vehicles, exhibiting favourable properties such as biocompatibility, drug loading and release, targeting, and cell uptake. In addition, click chemistry methods have been developed for surface modification of exosomes. Restriction of diffusion in the vitreous is a promising strategy to decrease drug clearance, potentially allowing for reduced injection frequency and delivery of small molecule drugs. To restrict diffusion, use of hyaluronan-binding domains to bind the omnipresent hyaluronan found in the vitreous is an encouraging strategy. However, there is a need to carefully select and optimize these hyaluronan-binding domains for their application in a nanoparticle-based drug delivery system. Of the multiple different hyaluronan-binding domains, peptides based on the B-(X7)-B motif appeared as a candidate that could be optimized using in-silico molecular docking techniques.

In this project, exosomes were isolated from retinal pigment epithelial cell culture using affinity capture and differential ultracentrifugation and characterized for their size, zeta potential, morphology, cell uptake, and drug loading abilities. Molecular docking was used to find and design peptides (based on the B-(X7)-B motif) with affinity to hyaluronan. Exosomes were conjugated with the candidate peptide

using click chemistry and then evaluated in an in-vitro diffusion cell model to evaluate the effect of peptide conjugation.

For both isolation methods, characterization indicated size distributions and mean diameter, negative zeta potential, CD63 presence, and round morphology, within the expected characteristics of exosomes. Of the two isolation methods, ultracentrifugation was deemed superior due to its reported ease of use, yield, and functionality. Fluorescently labeled exosomes qualitatively displayed time-dependent cell uptake into retinal pigment epithelial cells in culture. Given the biological function of exosomes as paracrine communicators, these results are expected. However, given the multitude of retinal cells affected in diabetic retinopathy, it might be more useful to quantitate exosome uptake in other retinal cell lines. Molecular docking revealed that slight modifications to the B-(X7)-B motif could result in greater affinity to hyaluronan. However, optimization is still needed to maximize hyaluronan-binding affinity. The conjugation chemistry was validated by use of a fluorophore. However, it was inconclusive as to whether peptide conjugation affected exosome diffusion within the diffusion cell model. Additional investigation studies and optimizations are required to elucidate the effect of peptide conjugation on exosome diffusion in the vitreous. This work will help in the development of both extended intravitreal drug delivery systems and exosome-based drug delivery systems.

# Acknowledgements

I would like to thank my supervisor Dr. Emmanuel Ho for his continued support and patience. I would also like to thank my advisory committee members, Dr. Lyndon Jones and Dr. Marianna Foldvari for providing me with valuable insight and discussion throughout the duration of my studies.

A special thanks to Yusheng Zhao and Dr. Praveen Nekkar Rao for their collaboration and assistance in the project. This project would not be possible without their considerable expertise in molecular docking and molecule design.

I am fortunate to have had wonderful lab mates: Yannick, Nehil, Jin, Sihan, Chuying, and Calvin. They provided me valuable discussion, assistance, laughs, and fun times - graduate studies would not have been possible without them. I was also fortunate to have the privilege to supervise Jennifer Bao, who contributed to this project.

Lastly, I would like to thank my family my friends for their love and support. This work would not be possible without them.

# Table of Contents

# List of Figures

# List of Tables

# List of Abbreviations

**A**

AA ..... amino acid

AFM ..... atomic force microscopy

**C**

CTAB ..... cetrimonium bromide

Cy3 ..... cyanine3

**D**

Da ..... daltons

DAPI ..... 4′,6-diamidino-2-phenylindole

DBCO ..... dibenzocyclooctyne

DG-UC ..... density gradient ultracentrifugation

DLS ..... dynamic light scattering

DNA ..... deoxyribonucleic acid

DR ..... diabetic retinopathy

DSP ..... dexamethasone sodium phosphate

**E**

EE ..... encapsulation efficiency

ELISA ..... enzyme-linked immunosorbent assay

**F**

FBS ..... fetal bovine serum

FC ..... flow cytometry

**H**

HA ..... hyaluronan

HDL ..... high-density lipoprotein

**L**

LDL ..... low-density lipoprotein

**N**

NHS ..... N-hydroxysuccinimide

NTA ..... nanoparticle tracking analysis

**P**

PBS ..... phosphate-buffered saline

PEG ..... polyethylene glycol

**R**

rcf ..... relative centrifugal force

RFP ..... red fluorescent protein

RNA ..... ribonucleic acid

RPE ..... retinal pigment epithelium

**S**

SD ..... standard deviation

SEC ..... size exclusion chromatography

SEM ..... scanning electron microscopy

STEM ..... scanning transmission electron microscopy

**T**

TEM ..... transmission electron microscopy

TRPS ..... tunable resistance pulse sensing

**U**

UC ..... ultracentrifugation

UPLC ..... ultra-performance liquid chromatography

**V**

VEGF ..... vascular endothelial growth factor

VH ..... vitreous humour

# Chapter 1: Introduction

## 1.1 Diabetic Retinopathy

Diabetic retinopathy (DR), amongst other complications, is a serious complication of diabetes that can result in vision problems or blindness. According to a literature review which surveyed 72 articles from 33 countries, the median prevalence of DR in diabetic patients is 27.9%.[1] DR is also the most prevalent cause of blindness in developed countries.[2]

The early stages of DR are termed non-proliferative DR. This stage is characterized by microaneurysms and other abnormalities in the retinal vasculature.[3] The disease progresses into a more serious stage termed proliferative DR, which is characterized by vascularization of the retina and breakdown of the blood-retinal barriers.[3] The precise mechanism in which hyperglycemia leads to retinal neovascularization is still unclear. It is known that hyperglycemia increases oxidative stress, which can lead to apoptosis of retinal cells and elevated vascular endothelial growth factor (VEGF) expression,[4] a pro-angiogenic factor that reduces retinal barrier function.[5] However, a recent review article highlighted that several related biochemical pathways may contribute to pathogenesis, including "increased polyol pathway, activation of protein kinase C, increased expression of growth factors such as VEGF and insulin-like growth factor-1, haemodynamic changes, accelerated formation of advanced glycation endproducts, oxidative stress, activation of the renin-angiotensin-aldosterone system, and subclinical inflammation and capillary occlusion.[6]" Clearly, DR is complex, and successful treatment will likely require targeting multiple axes.

There are several imaging techniques that are used to diagnose DR. Fundus photography produces images of the posterior structures of the eye, allowing physicians to identify areas with neovascularization.[7] Fluorescein angiography is performed by systemically injecting sodium fluorescein, followed by making fluorescence measurements using a fluorescence-modified fundus camera.[7]

Depending on the spread and intensity of fluorescence, varying conclusions can be made regarding retinal vascular integrity.[7]

Treatment of DR is attempted through three modalities or the various synergistic combinations of photocoagulation, vitreoretinal surgery, and pharmacotherapy.[8] Photocoagulation uses laser energy to cauterize retinal blood vessels, reducing neovascularization and reducing rates of vision loss.[9,10] Vitreoretinal surgery is indicated for DR when there is vitreous hemorrhage or retinal detachment causing vision loss.[8]

Pharmacotherapy of DR is attempted through use of intravitreal injections of anti-VEGF agents or steroids. Currently, anti-VEGF agents are currently the gold-standard for pharmacological treatment of retinal neovascularizarion.[8,11] Commonly used anti-VEGF agents include, bevacizumab, ranibizumab, and aflibercept.[8] To mediate their effects, the anti-VEGF agents bind and neutralize VEGF produced by retinal cells.[11] Steroids, such as dexamethasone, fluocinolone, or triamcinolone, may be alternatively used when anti-VEGF agents are contraindicated, although they are associated with increased risk of intraocular pressure.[12] To mediate their effects, the steroids block VEGF signaling or decrease VEGF expression.[13] Ocular anatomy and ocular pharmacokinetics, however, still present as challenges and severely limit the scope and effectiveness of pharmacotherapies that can be applied to posterior ocular diseases.

## 1.2 Ocular Anatomy

Ocular anatomy (Figure 1) plays a large role in the pharmacokinetics of the various routes of administration. The eye is mostly surrounded by a fibrous tissue known as the sclera.[14] The exposed part of the eye is protected by the conjunctiva, a tissue layer which also covers part of the sclera.[14] The anterior of the eye consists of, starting from the outside, the cornea, anterior chamber, lens, and posterior chamber.[14] The cornea is a multi-layered cellular barrier covered by a tear film.[14] The lacrimal apparatus is responsible for secretion and drainage of the tear film. The proximal layer of the tear film is mucinous in nature, and the cornea surface is considered a mucus membrane.[14] The ciliary body consists of the

ciliary muscle which controls the shape of the lens, and the epithelial cells which secrete the aqueous humour, which fills the anterior and posterior chamber. Aqueous humour flows from the posterior chamber to the anterior chamber and then is drained into Schlemm's canal.[14]

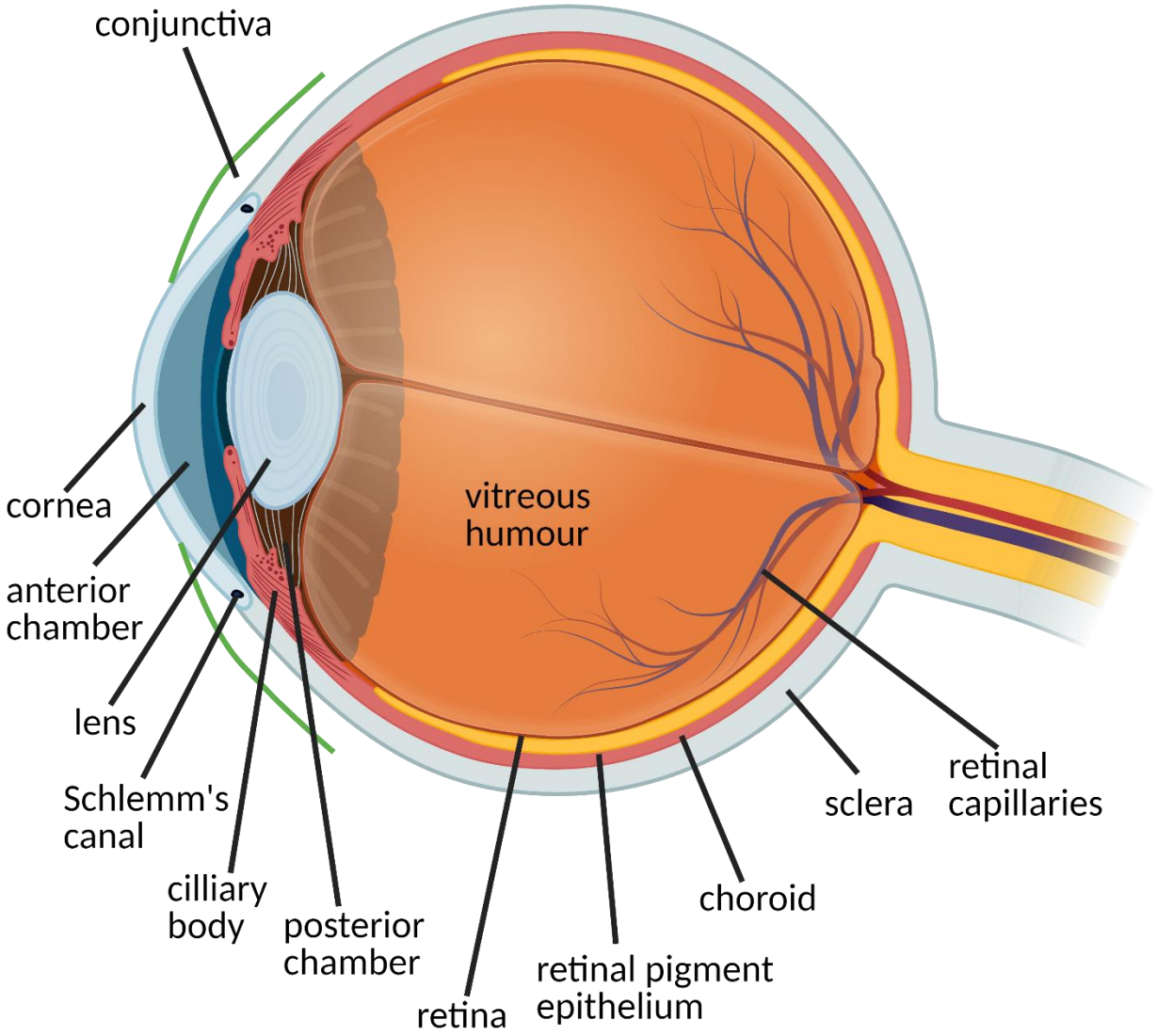


Figure 1. Structure and anatomy of the human eye. Anatomical structures relevant to retinal drug delivery are labeled. Created with BioRender.com.

Further inward is the posterior segment of the eye, which includes the vitreous humour (VH), retina, and choroid.[14] The VH is a clear, jelly-like fluid that occupies two thirds of the eye. The major biochemical components of the VH are collagen and glycosaminoglycans, which form mesh networks to support the structure of the VH. It is estimated that the pore size of the collagen networks in bovine VH

is 550 +- 50 nm.[15] Of the glycosaminoglycans, hyaluronan (HA) and chondroitin sulfate represent 92% and 8% in healthy human VH, respectively.[16] HA is a high molecular weight anionic glycosaminoglycan that constitutes a major portion of extracellular matrices, including the VH. HA consists of repeating disaccharides of D-glucuronic acid linked in a β(1-4) glycosidic bond to N-acetyl-D-glucosamine.[17] Disaccharides are linked to each other by β(1-3) bonds. HA found in the VH has an average molecular weight of 2-4 million Daltons (Da), depending on source.[18] In the VH, HA is produced and secreted by hyalocytes which are distributed towards the periphery of the VH.[19] HA is found at concentrations of 100-400 μg/mL in the human VH, with highest concentrations in the posterior VH near the retina.[19] There are slight differences in VH composition between humans and the commonly used animal models, but in general, the compositions are quite similar.[19]

The retina is composed of several cell layers which serve different roles. The neural retina consists of photoreceptors which transmit signals to bipolar cells, which transmit signals to retinal ganglion cells.[14] Axons of retinal ganglion cells bundle to form the optic nerve.[14] Damage to the neural cells is the cause of DR-induced vision problems. Like other neural cells, cells of the retina require large amounts of energy, oxygen, and thus also blood supply.[20]

The choroid is a highly vascular tissue that supplies blood from the ophthalmic artery to the photoreceptor cells of the outer retina.[20] The retinal pigment epithelium (RPE), the outermost layer of the retina, is a tight cellular monolayer which serves as a barrier between the outer retina and the choroidal capillaries.[14] Due to presence of tight junctions, only diffusion of small molecules (< 3 nm) is significant.[21] Other than acting as a barrier, RPE cells also secrete molecules to support other retinal cells.[22] Breakdown of the RPE followed by leakage, causing macular edema, is one contributor to the complications of DR.[23]

The other source of blood supply to the retina are the retinal capillaries, which originate from a separate branch of the ophthalmic artery.[14] The retinal capillaries are referred to as the inner blood-retinal barrier, as they supply blood to the inner retina.[14] In DR, angiogenesis of retinal capillaries can disrupt cells of the neural retina and affect vision.

## 1.3 Nanotechnology

Nanotechnology describes technology designed within the nanometer range (approximately less than 100 nm). Since its invention, nanotechnology has greatly improved various applications in electronics, energy, and medicine. In medicine, nanotechnology has been used in organ imaging, regenerative medicine, and to improve drug delivery. Nanoparticles are carefully and precisely designed carriers that can facilitate better abilities to deliver drug to target, tissues, organs, cells, or even organelles. In general, nanoparticles can improve drug solubility, facilitate controlled release, and protect cargo from degradation.

Nanoparticles are formed as a result of the system's means of decreasing unfavorable interactions between the solvent (usually water if hydrophilic) and hydrophobic molecules. The key mediator to decrease these unfavorable interactions are amphiphilic molecules, consisting of both a hydrophobic and hydrophilic region. Using micelle formation in water as an example, upon achieving a high enough concentration of amphiphilic molecules, the amphiphilic molecules will spontaneously arrange themselves to form a sphere with the hydrophilic regions of the molecules pointing outwards towards the solvent and the hydrophobic regions pointing inwards forming a core in which any hydrophobic molecules such as drugs will reside.

Common nanoparticles include polymer-based nanoparticles, metallic nanoparticles, quantum dots, hybrid nanoparticles made from multiple material types, and liposomes. Recently, there has been interest in the use of biologically derived nanoparticles called exosomes.

## 1.4 Retinal Drug Delivery and Pharmacokinetics

Topical drug formulations (e.g. eye drops) have poor penetration, low retention time, or require frequent re-administration, thus are limited to anterior segment diseases and can reduce patient compliance. For the corneal route of absorption, the drug must penetrate through the corneal epithelium while avoiding rapid clearance by conjunctival drug absorption or lacrimal apparatus.[18] It is estimated that drainage by the lacrimal apparatus washes away most topical formulations within 30s.[24] Some novel formulations have

taken advantage of mucoadhesive materials or gel-like materials to reduce drainage by the lacrimal apparatus. The fraction of administered dose that can penetrate into the aqueous humor is rapidly cleared by aqueous humor outflow.[18] Aqueous humor flows into the trabecular and uveoscleral pathways with a turnover time of approximately 86 mins.[25] For the non-corneal route of absorption, the drug passes through the conjunctiva, sclera, and choroid on its way to the retina.[18] For drug delivery to the retina from topical administration, focusing on the non-corneal route appears more promising.[18] However, bioavailability of topically administered drugs, as measured in the posterior regions (retina, choroid, or VH) is negligible.[18]

The periocular injection route describes injections to areas surrounding the eye. Drugs injected into periocular regions will diffuse across the sclera into the choroid, and then from the choroid into the retina.[18] However, drugs are still rapidly cleared into systemic circulation and may not be able to permeate the RPE at therapeutic concentrations.[18] Suprachoroidal injections describe injections into the choroidal region, beneath the sclera. The pharmacokinetics and also limitations of this route of delivery are similar to that of periocular injections. Sub-retinal injections describe injections to space between the neural retina and the RPE. While great in theory, this method is technically demanding and not feasible for widespread clinical application as of yet.[18]

Intravitreal injections are the only viable pharmacokinetic route, and thus are the gold-standard for pharmacological treatment of retinal neovascularization disease. The anti-VEGF agents are large protein drugs, and thus have longer half-lives in the VH due to restricted diffusion. Anti-VEGF agents have half-lives of about a week, and individuals are injected monthly. This is possible as anti-VEGF proteins can be administered at high concentrations with no side effects. Most small molecule drugs, do not share this property, and thus are currently unfeasible for use as they are rapidly cleared below therapeutic concentrations.[26] For example, use of small molecules such as dexamethasone is only effective when formulated for extended release through the use of nanoparticles or implants.[18] Elimination from the VH can occur partially through outflow into the aqueous humor, or primarily through diffusion across the blood-ocular barriers.[26] Alternatively, metabolism by enzymes found in RPE cells can contribute to

elimination.[27] However, intravitreal injections can inherently cause complications such as endophthalmitis, intraocular inflammation, and retinal detachment.[28] Moreover, the monthly hospital visits can disrupt personal life and affect compliance, directly affecting success of treatment,[29,30] thus it is necessary to develop long-lasting formulations to reduce injection frequency and allow for delivery of drugs with less favorable pharmacokinetics.

Previous research has proposed that increased diffusion is beneficial to retinal drug delivery,[15] as drugs or nanoparticles can diffuse to the site of action(s). However, when designing a system to reduce injection frequency, restricting or slowing down diffusion may be more beneficial.

### 1.4.1 Restricting Diffusion in the VH

Modulation of the drug or macromolecule size with poly-ethylene glycol (PEG) is one approach to decreasing its clearance rate after intravitreal injection.[31] However, there lacks a quantitative understanding on how drug size might affect distribution or clearance.[31] Abicipar pegol is a PEGylated anti-VEGF agent which provided a slightly longer duration of action than ranibizumab in a rabbit model of retinal vasculopathy.[32] Zimura is a PEGylated complement C3-inhibitor proposed to treat age-related macular degeneration.[33] In monkeys, a single intravitreal injection resulted in steady concentrations (200 nM month 1, 100-120 nM month 3) for up to 90 days.[33] However, there are safety concerns as clearance of PEG from the eye is still unknown.[31]

Use of HA-binding structures is an alternative strategy to decreasing VH clearance rate, as HA is a major structural component of the VH. An anti-VEGF agent has been conjugated to naturally occurring HA-binding sequences found in human proteins.[34] In a rabbit model of retinal vascular leakage, one of the modified anti-VEGF agents maintained high efficacy even after 4 weeks post-injection, while the un-modified anti-VEGF agents showed a large decrease in efficacy by 3 weeks.[34] Cholesterol dextran nanoparticles were conjugated with short peptide-PEG conjugates of under 5 amino acids. The peptides were derived from sequences found in natural intraocular peptides and had 2 or 3 arginine residues.

Amino-PEG8 was used to improve conjugation yield to the nanoparticles.[35] In a rabbits, one of the peptide-conjugated nanoparticles had over 3x the half-life of unconjugated nanoparticles.[35]Although not directly evaluated, HA-binding is the likely mode of action.

### 1.4.2 HA-Binding Domains

HA, under physiological conditions, is anionic in nature. Several native HA-binding domains have been discovered, including the link module,[36] double arginine motif,[37] and B-(X7)-B motif.[38] The binding interactions are largely achieved by interactions between cationic amino acids to anionic groups on HA. The link module is a protein consisting of approximately 100 amino acids (AA) with two disulfide bridges that confer the secondary structure necessary for activity.[39] The double arginine motif is a pair of adjacent arginine AA that binds weakly through electrostatic interactions, but binds more weakly than the B-(X7)-B motif.[37] HA-binding domains that rely on series of adjacent cationic AA likely have the weakest interaction, considering that poly-lysine peptides are not able to inhibit binding of the B-(X7)-B motif.[40] This B-(X7)-B consists of two basic (arginine or lysine) AA, flanking seven non-acidic AA. It is believed that the seven spacing AA also play an important role in binding to HA.[38]

Ideally, a HA-binding domain would be specific, cheap, have no immunogenicity, and minimally alter the nanoparticle of interest. A peptide based on the B-(X7)-B motif is therefore an ideal candidate, as it exhibits strong and specific binding, is cheap to produce, and is of small size. Highly cationic peptides may also mediate non-specific binding and toxicity while larger peptides or proteins can introduce issues with immunogenicity, be cost-prohibitive, or alter nanoparticle morphology. While the B-(X7)-B motif alone is found to bind to HA, sequence optimization is needed as the exact composition of the internal sequence and flanking sequences may affect HA-binding.[38]

## 1.5 Molecular Docking

Molecular docking is an “in-silico” technique with high value to design and develop small molecules, proteins, and peptide libraries that can bind and interact with desired molecular targets such as

enzymes and proteins.[41–43] Computational molecular docking can significantly reduce the time and cost involved in discovering new drug candidates and to optimize lead molecules and is frequently used in the pharmaceutical industry.[41–43] The basic principle of molecular docking is based on the classic lock-and-key model where the compound/molecule libraries interact with receptor active sites or binding sites to investigate their application as enzyme inhibitors. The goodness-of-fit is evaluated by measuring 1) ligand-receptor complex energies and 2) scoring functions. Many efficient computational algorithms have been developed for molecular docking studies and computational software is commercially available. Molecular docking algorithms have evolved over the years to include both rigid and flexible receptors for docking purpose. Ligand or molecular libraries such as small molecules, peptides, oligonucleotides, or polymer fragments can be built in 3D and can be docked virtually. The 3D structures of molecular targets can be obtained through structural databases such as the protein data bank (rcsb.org) which includes X-ray, NMR, or electron microscopy based structures.[44] If the 3D structure of the molecular target is not available, it can be built using homology modeling or by using the tools that are typically available in many computational software programs.

## 1.6 Exosomes as Drug Delivery Vehicles

Subsections 1.6.1 and 1.6.2 are revised from the review article published in the Journal of Controlled Release. https://doi.org/10.1016/j.jconrel.2020.10.020

### 1.6.1 Overview

Exosomes are spherical lipid-bilayered particles released from cells and are classified under extracellular vesicles which also includes microvesicles and apoptotic bodies, all of which differ in morphology and biogenesis. For example, microvesicles (50 – 1000 nm) and apoptotic bodies (50 – 5000 nm) are formed from the budding of the plasma membrane.[45] Exosomes are 40 – 100 nm diameter particles formed and released from the endosomal pathway (Figure 2), which begins as inward budding of the plasma membrane to form the endosome, a membrane-bound organelle.[45] The endosome will then

invaginate to form intra-luminal vesicles during endosomal maturation into a multivesicular body.[46] Following this, the multivesicular body can fuse with the plasma membrane to release its vesicular content as exosomes.[46] Several markers involved in the formation of intraluminal vesicles, as we highlight later, are used as markers of exosome enrichment.

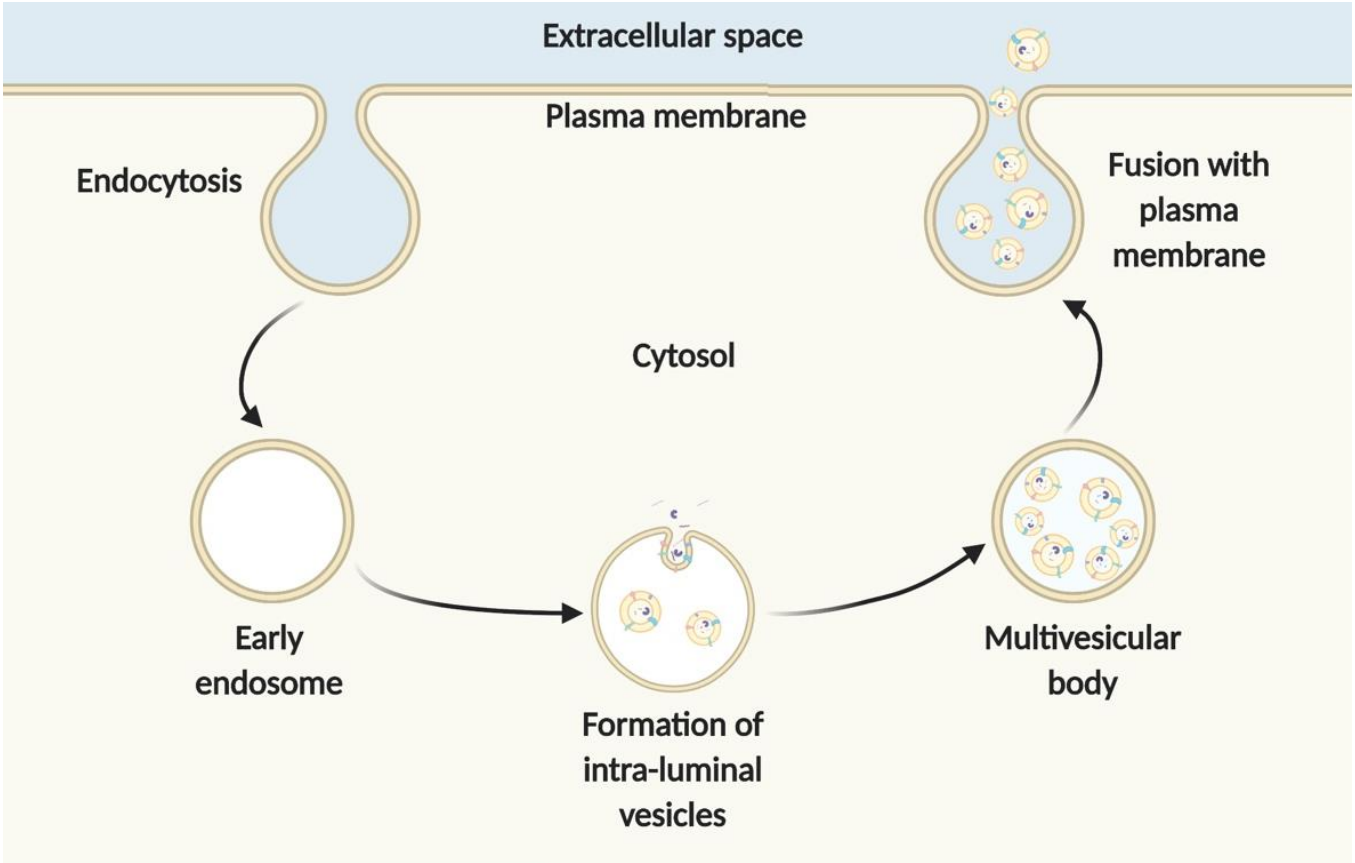


Figure 2. Exosome formation and release from the endosomal pathway. Exosome biogenesis begins with endocytosis to form the endosome. The endosome invaginates to form intra-luminal vesicles during its maturation process into a multivesicular body. The multivesicular body fuses with the plasma membrane to release the vesicles, termed as exosomes. Created with BioRender.com.

Exosome release was initially hypothesized to be a process to expel waste.[47] However, exosomes are now known to be important mediators of intercellular communication.[48] During exosome formation, biomolecules including cell-targeting moieties, cell adhesion moieties, coding and non-coding ribonucleic acid (RNA) can be packed within the lumen or lipid bilayer, contributing to the many functions of exosomes.[48] Thus, the contents of an exosome are dependent on the phenotype of the donor cell. The structure of an exosome most resembles a unilamellar liposome, consisting of an amphiphilic lipid bilayer

surrounding an aqueous core. In liposomal drug delivery systems, hydrophobic drugs distribute within the bilayer while hydrophilic drugs distribute within the lumen.[49] Due to their similarities, it is expected that exosome drug delivery systems will exhibit similar characteristics as liposomes. For these reasons, it is believed that by carefully selecting the exosome source, exosomes can be used as highly specific drug delivery systems. Over the past few years, there has been several examples demonstrating pre-clinical success in using exosomes as drug delivery systems for a multitude of therapeutic applications. For example, exosome encapsulation was found to improve the solubility, stability, and anti-inflammatory properties of curcumin.[50] Furthermore, the exosomal formulation was superior to the liposomal formulation in protecting mice against lipopolysaccharide challenge.[50] Paclitaxel-encapsulated exosomes were also found to exhibit superior antineoplastic effects than free paclitaxel in a mouse model of lung carcinoma.[51] Exosomes derived from brain endothelial cell culture was able improve the penetration of doxorubicin and paclitaxel across the blood-brain barrier in zebrafish embryos.[52] Surface-functionalized mesenchymal stem cell exosomes loaded with curcumin injected intravenously were able to distribute into ischemic brain tissue.[53] Macrophage-derived exosomes loaded with catalase protected against neuroinflammation in a mouse model of Parkinson's disease. In addition, targeted exosomes have been used for the delivery of small-interfering RNA to the brain in mice.[54]

Exosomes, being cell-derived, are regarded to have excellent biocompatibility. In our scope of our research, ocular-derived exosomes are safe when administered to the eye.[55] ARPE19 cells are a cell line derived from primary human RPE cell culture.[56] Exosomes from healthy ARPE19 cells inhibited angiogenesis in vitro,[57] reflecting the concept that many exosomes have intrinsic properties. In addition, ARPE19 derived exosomes, based on the function of exosomes, likely possess molecules that enhance or mediate the uptake or binding to other retinal cells.

### 1.6.2 General Techniques in Exosome-based Drug Delivery

#### 1.6.2.1 Source Selection

The first step in the design process is to determine the cellular source of exosomes. For human cell-derived exosomes, cell culture is the most accessible source. The International Society for Extracellular Vesicles has provided recommendations for a framework on how to work with cell culture exosomes.[58] If the biochemical components of the exosomes are important for drug delivery, such as for specific cell targeting, then cell phenotype must be controlled and monitored carefully. Passage number has been shown to alter cell and exosome content but not exosome production rate, at least in mesenchymal stem cells.[59] Cell confluency can affect phenotype and thus potentially the exosomes released. For example, cells at maximum confluency may have altered metabolism which might alter exosome release kinetics.[60] It is recommended that passage number and confluency are reported to increase reproducibility.[58] Cells, in the process of dying, may release apoptotic bodies, which may be co-isolated with exosomes depending on the isolation method. It is in the best interest to have a low number of dead or dying cells at the time of harvest. An acceptable cut-off will have to be determined experimentally individually, based on the downstream applications. Fetal bovine serum (FBS), used commonly to aid in cell culture growth, contains exosomes which may be co-isolated and misidentified for the target cell's exosomes.[58] For cells that require serum supplemented media, exosome-depleted FBS is used as a substitute for FBS.[58] FBS can be depleted of exosomes by various methods such as extended ultracentrifugation or filtration,[61] or can be purchased from commercial vendors. However, it is important to note that exosome-depleted FBS is not completely void of bovine exosomes. Moreover, presence of plasma lipoproteins in FBS may present as an issue depending on the downstream isolation method. To ensure absence of FBS exosomes or lipoproteins, some cell lines can be grown in serum-free media, but the feasibility and validity of this must be determined on a case-by-case basis.

To upscale exosome production for cell culture, advanced cell culture systems such as hollow fiber cell bioreactors and stirred tank bioreactors can be used.[62] Hollow fiber bioreactors comprise of small

semi-permeable fibers that greatly increase the surface area on which cells can attach to, allowing media to continuously flow through. Fresh media is flowed through the system without a need for passaging, while exosome-containing media can be harvested. It has been suggested that the exosomes collected from bioreactors are more representative of exosomes that may be found in live tissue, as cells are grown in 3D structures as opposed to a monolayer.

#### 1.6.2.2 Isolation

Based on current technologies for exosome isolation, there is no method that can achieve a pure isolate containing no other components. Thus, for the purpose of this thesis, exosome isolation will be used to refer to a technique to enrich exosomes relative to the other biological macromolecules. For drug delivery, this isolation method ideally has the following key characteristics: high yield, high purity, and high scalability. The isolation method must also preserve vesicular structure. With the currently available methods, there are trade-offs that exist between purity, yield, scalability, and preservation of vesicular structure. It naturally follows from the limitations of the current isolation techniques, that purity considerations may not be considered enough, which may hinder the progress of exosome-based drug delivery into the clinic. Considering that the lipoproteins that are commonly isolated with exosomes are also being investigated themselves as drug delivery vehicles,[63] the extent to which the non-exosome biological macromolecules contribute to the success of exosome drug delivery is unknown.

Differential ultracentrifugation (UC) was the first method used to isolate exosomes,[47] and is still considered the popular method used to isolate exosomes due to its simplistic protocol and use in most literature. By stepwise increase of relative centrifugal force (rcf), centrifugation can remove unwanted contaminants at each stage of the process. For example, centrifugation at 200 rcf, 2,000 rcf, 20,000 rcf, and finally 100,000 rcf will precipitate cells, large debris, microvesicles/apoptotic bodies, and finally exosomes, respectively. However, UC is also a technique used to isolate lipoproteins.[64] From cell culture (using media with 10% exosome-depleted serum), one group estimated that 20% of their isolate was not

exosomes.[65] If using a prolonged UC protocol (~4 hrs) there is further risk of contamination by soluble proteins.[66] It is possible that the centrifugal forces on exosomes during repeated UC can cause rupture of the exosomal membrane.[67] UC is, however, the most well established method to isolate exosomes, and can serve as a useful initial comparator for future methods, or as a downstream recovery method with high yield.

Density gradient UC (DG-UC) is based on the principle of setting up an increasing density gradient of solutions from the top of the tube to bottom. Following centrifugation, exosomes will sediment into the layer matching exosome density, while other contaminants of other densities will be separated into other layers. Among physical-based exosome isolation methods, DG-UC is one of the best in terms of purity, yield, and preservation of vesicular structure. However, high-density lipoprotein (HDL) and low-density lipoproteins (LDL) contamination of the exosome-containing fraction has been observed.[68] One group estimated that their exosomes were co-isolated into the same fraction as HDL, at a ratio of 1:100 (exosome:HDL).[64] With an optimized protocol, one group was able to minimize lipoproteins through use of extended DG-UC.[69]

Size exclusion chromatography (SEC), also known as gel filtration chromatography or gel permeation chromatography, is a chromatography technique in which a column with porous beads is used to retain particles smaller than the pore size while rapidly eluting particles larger than the pore. Exosomes are 40 – 100 nm in diameter, while most proteins are below 10 nm. By first using centrifugation to remove larger debris, followed by SEC using appropriately sized beads, exosomes can be isolated from proteins. Beads that have been used to isolate exosomes from protein include Sepharose CL-4B, Sephacryl S-400, and Sepharose CL-2B.[70–72] The apparent pore size distribution of these SEC beads are 42, 31, and 75 nm, respectively.[73] However, larger protein complexes such as some lipoproteins (LDL, very low-density lipoproteins, and chylomicrons) overlap in size with smaller exosomes. Thus, there is a trade-off when selecting bead size – large bead sizes will remove more lipoproteins but lose smaller exosomes, while small bead sizes will allow for isolation of smaller exosomes but also lipoproteins. Furthermore, bead

sizes themselves follow a distribution and mean bead size is not a hard cut-off for particle removal.[73] SEC also requires that the input sample volume be much smaller than the column volume, otherwise the sample will elute unevenly and decrease separation efficiency.[74] Furthermore, the elution process will invariably lead to a sample dilution due to diffusion and may need to be concentrated post-isolation by another method, leading to decreased yield. SEC does, however, have several advantages. As the exosomes are not subject to any harsh physical interaction, the vesicular structure is well preserved.[71]

Filtration describes a broad variety of techniques that use membranes with specific pore sizes to selectively retain or elute particles of certain size. In direct flow filtration, the membranes are setup perpendicular to the flow. Due to the force used to push particles through the membrane, the retentate may "trapped" within the membrane or excess force may result in larger particles being forced across the membrane.[75] In tangential flow filtration, the flow is setup parallel to the membrane. In one example, the pressure was carefully controlled to minimize exosome loss through membranes due to excessive force.[75] Continuous recycling of the retentate to pass over the membrane continuously greatly improves isolation efficiency when compared to direct flow filtration. In another study, tangential flow filtration was superior to UC in scalability and time consumption (~1 hour).[76]

Affinity capture describes a technique in which exosome capture molecules are attached to an easily removable carrier (e.g. magnetic beads). Upon interaction of the capture molecule with the exosome antigen, the exosome attaches to the carrier bead to form a complex which can be magnetically separated from the rest of the sample. The properties of the interaction between the capture molecule and the antigen are highly important to the downstream applications. For example, using an antibody as the capture molecule (e.g. against CD63) can isolate exosomes with high purity, which is very good for proteomics, lipidomics, or RNAomics.[77] However, breaking the interaction between an antibody and an antigen requires harsh conditions that will destroy the vesicular structure of the exosomes and is counterproductive to exosomal-based drug delivery. On the other hand, by taking advantage of a more easily reversible

reaction (e.g. Tim4-phosphatidylserine), pure exosomes in vesicular form can be recovered, although with possibly lower yield.[31]

#### 1.6.2.3 Characterization

Following isolation, exosome samples should be thoroughly characterized by multiple methods to validate the isolation method. The most common characterization methods can be classified as marker, biophysical, or imaging-based, each with their own purpose.

Protein/marker-based characterization methods can be used to ensure that the isolated sample does contain a high level of exosome markers and a low level of potential contaminants. Total protein assays can be used to quantify total exosome protein content, however, this method does not discriminate between exosomal proteins and non-exosomal proteins, which is concerning as non-exosomal proteins are co-isolates of many exosome isolation methods. Total protein can however, be used with other characterization methods as an estimation of sample purity (e.g. particle:total protein ratio, CD63:total protein ratio).

Due to their endosomal origin, exosomes from most sources will contain membrane proteins or intraluminal proteins which were involved in processes of endosomal formation. The International Society for Extracellular Vesicles has put forth extensive recommendations for marker-based exosomal characterization.[58] Characterization of these protein markers can be easily done using Western Blot or enzyme-linked immunosorbent assay (ELISA). Although important, positive indicator of exosome markers does not indicate that the isolated sample is in colloidal form – exosome lysis may have occurred during the isolation or storage process.

Atomic force microscopy (AFM) is an imaging technique that relies on the measurement of force between the probe and sample, to produce a topological map of the sample. From this map, sample height and diameter can be estimated. Using AFM, exosome diameter is generally found to be within the expected range of exosomes (40 - 100 nm).[79–82] Although sample height is one of AFM's unique measurements,

care must be taken when drawing conclusions. AFM imaging of exosomes "in air" will estimate exosome height to be approximately 20 nm,[79,80] which is lower than the expected range (40 - 100 nm) if exosomes are assumed to be spherical, likely due to sample drying. It has been suggested that measuring exosomes in a more physiological environment by using AFM "in liquid" produces more relevant images, although height data still does not indicate perfect spherical morphology.[83,84] It is limited as a surface technique, in that only surface elements can be captured. The advantage AFM has over other techniques is that it can be used to determine height, and other mechanical features (compression, deformation).[85]

Electron microscopy is an imaging technique adapted for greater magnification and resolution than optical microscopy. The most used modalities are scanning electron microscopy (SEM) and transmission electron microscopy (TEM). Exosome morphology under electron microscopy appears round, with a cup shape morphology, likely attributed to a collapse of structure following desiccation. The size distribution is within the expected distribution confirmed by other techniques. One of the limitations of electron microscopy is that there is high variability in image selection, dependent on the operator. One group evaluated imaging of exosomes using different TEM protocols and found that operator image selection is a huge factor in image quality.[86] Questions arise as to whether the selected area is representative of the whole sample. Thus, it can be risky to draw conclusions about sample concentration and size distribution from electron microscopy. Similarly, there are limited conclusions that can be drawn regarding sample purity. It was suggested that electron microscopy should serve solely as a confirmatory technique to determine the presence of exosomes.[86] A larger concern about using electron microscopy for exosomes, is how it can be accurately confirmed that the spherical object in the image is actually an exosome, as certain lipoproteins are also spherical objects with overlap of exosome size distributions. Immunogold electron microscopy can be used to selectively stain certain markers on exosomes, and can be a very useful tool to confirm presence or absence of specific markers on images.[87]

Dynamic light scattering (DLS) is a biophysical technique that measures fluctuations in the light scattering caused by small particles exhibiting Brownian motion. Based on fluctuations of light scattering,

correlations to hydrodynamic radius can calculated. DLS has several notable limitations for the characterization of exosomes. Firstly, it requires higher concentrations of particles, which may be challenging to prepare for exosomes. Secondly, particles scatter light proportional to $r^6$, thus larger particles can drastically influence the intensity distribution, resulting in the exosome population being masked. Thirdly, the fluctuations of the entire sample are captured, which makes DLS inherently unsuited for polydisperse samples (exosomes).[88] Fourth, DLS is unable to accurately estimate particle concentration. Fifth, particles with low scattering properties (exosomes) can make readings inaccurate.[88]

Flow cytometry (FC) is biophysical technique that passes individual single cells in front of a laser and detects scattered light or emitted fluorescence. The lower detection limit (200 – 500 nm) of conventional FC limits its use in detecting free exosomes.[89,90] FC optimized for small particles can be used to detect exosomes.[90–92] However, the lower limit of detection is still approximately 100 nm, which suggests insufficient sensitivity. Decreasing the laser wavelength to 405 nm has been suggested to improve instrument sensitivity to exosomes.[92,93]

Nanoparticle tracking analysis (NTA) is a recently developed biophysical technique which relies on the same fundamental principles as DLS. However, it differs to DLS in that a microscope is used to capture the Brownian motion of individual particles. Many NTA machines also have fluorescence capability. By changing the laser and/or filters, many different fluorophores can be used to tag particles or proteins of interest. For example, fluorophore conjugated antibodies can be used to label exosomes for fluorescent NTA.[94] However, in practicality, only strong fluorophores resistant to photobleaching can be feasibly used. One concern is regarding the limit of detection of the NTA, which is reported by manufactures as ranging from approximately 10 – 1000 nm. The lower limit is only achievable when measuring particles with high scattering index (e.g. metallic nanoparticles).[95] Exosomes range from 40 – 100 nm and are of low scattering index, raising the concern that exosomes on the lower end of the size range will not scatter sufficient light to be detected.[95] One of NTA's largest criticism is the large variability in the pre and post-processing settings can influence measured results. For example, most NTAs have

options to change increase camera sensitivity and to change the detection threshold for a particle (number of pixels required for software to identify signal as particle). The results can greatly vary depending on the settings.[96] Moreover, there are no set settings recommended by manufacturers or leaders in exosome researchers to aid in standardization. Thus, when using NTA for exosomes, it is critical to be consistent with settings and report all measurement parameters. Despite limitations, NTA appears to be the most versatile, reliable, easy to use technique for the biophysical characterization of exosomes.

Tunable resistance pulse sensing (TRPS) is a recently developed biophysical technique based on the passing of single particles through a nano-scale pore. As the particle passes through the pore, the magnitude, duration and frequency of resistance pulses is detected and used to determine size, zeta potential, and concentration. It has been reported that exosome size distribution and particle concentration as measured by TRPS more closely resembles the true distribution when compared to NTA. With TRPS, there is a trade-off between system stability (pore clogging) and system sensitivity to smaller exosomes.[97] Frequent pore clogging of exosome samples has been noted as a challenge to making measurements.[90,97]

#### 1.6.2.4 Storage

If exosomes are to be used as drug delivery vehicles, they must demonstrate stability. The pre-isolate, isolate, and downstream formulations must be stable as well. For exosomes, stability can be defined as resistance to aggregation, loss of structure, and protein degradation. Thus, to evaluate exosome stability, multiple methods should be employed. Quantifying levels of surface markers such as CD63 or CD81 can be used to determine if protein degradation has occurred. For drug delivery applications, characterization of colloidal stability of exosomes is highly important, and this is best evaluated by measurement of zeta potential, size distribution, and concentration. While electron microscopy is the only technique that can physically visualize morphology, electron microscopy images are highly operator dependent,[86] and may not accurately represent the entire sample.

Storage parameters have a large influence on sample stability. Temperature, time, and freeze-thaw cycles are by far the most commonly evaluated storage parameters. Osmotic pressure and pH are less studied but also have an important impact on stability. However, there have been conflicting reports on the optimal stability parameters due possibly to differing methods.

Exosomes exhibit size decrease as measured by NTA when stored for a couple of days at both 37°C and 4°C, but minimal size change is observed after multiple freeze-thaw cycles at -20°C.[88] Exosomes stored at 4°C and -80°C have also been observed to result in an increase in size as measured by DLS compared to freshly isolated exosomes.[98] Exosomes stored at -80°C also exhibited lower absolute zeta potential, possibly contributing to the increased aggregation observed using TEM.[98] Vesicles stored at 20°C or 4°C exhibited time-dependent decrease in concentration as determined by FC, but not for samples stored at -20°C or -80°C for up to one month.[99] Exosomes were resistant to freeze-thaw cycles in liquid nitrogen when supplemented with 1 mg/mL albumin.[99] Storage at -20°C led to time-dependent increase of size, but this was less noticeable at -80°C.[99] There was no difference in vesicle morphology when imaged by TEM.[99] Trehalose has also been used as a cryoprotectant in the lyophilization of exosomes.[100] Exosomes lyophilized in trehalose-supplemented phosphate-buffered saline (PBS) did not differ in polydispersity index (DLS) when compared to exosomes stored at -80°C, but exosomes lyophilized in PBS had significantly higher polydispersity index compared to the other storage conditions.[100] In addition, protein content and protein activity were similar in exosomes lyophilized in trehalose-supplemented PBS and exosomes stored at -80°C.[100] Repeated freeze-thaw cycles of exosomes in PBS caused a slight increase in particle concentration and the standard deviation (SD) of size (NTA), but not with exosomes in trehalose-supplemented PBS.[101] Exosomes measured in trehalose-supplemented PBS exhibited lower mean size, lower SD of size, and increased particle concentration, all of which were used to suggest that trehalose decreased exosome aggregation.[101] Exosomes stored at pH of 4 or 10 exhibited greater loss of exosomal protein and exosome concentration than those stored at pH of 7.[102] Interestingly, storage at 37°C and 60°C for 24 hrs was not as destructive to exosome concentration when compared to freeze-thaw

cycles.[102] However, the results of the study are limited by their choice of isolation method, which is known to co-precipitate proteins and lipoproteins along with exosomes, which may distort concentration measurements due to large presence of non-exosome particles. In addition, there was no mention of the agents used to change pH or their buffering capabilities.

Due to differing cells types, isolation methods, and characterization methods, it is challenging to find harmony amongst the current scientific literature. Like other biological samples, exosomes should be frozen (-20°C or -80°C) or lyophilized long-term (>1 week) and only stored at 4°C for very short periods (< 48hrs). Aliquots should be made to minimize need for freeze-thaw cycles. Storage at neutral pH with buffering capability and physiological osmotic pressure currently appears as most suitable. Characterization methods should be used frequently to evaluate exosome stability.

### 1.6.3 Drug Delivery Modifications

#### 1.6.3.1 Drug Loading

There is a plethora of strategies that have been employed to load drugs into exosomes. Pre-loading of exosomes can occur when the drug is introduced into the environment of the parent cell, which then incorporates the drug into the exosome during the biogenesis process. This strategy allows for incorporation of a variety of cargo type, including nucleic acids, small molecules, proteins expressed from messenger RNA, and etc.[103]

Post-loading of exosomes after isolation has far more varied techniques, most of which involve membrane permeabilization. For example, a recent review highlighted strategies including direct co-incubation, sonication, electroporation, freeze-thaw cycles.[103] In direct co-incubation, the drugs and exosomes are incubated together for a period of time. This strategy tends to be suited to hydrophobic compounds of smaller size. Sonication uses mechanical agitation, causing transient disruptions in the exosomal membrane in the form of small pores, which then may facilitate diffusion of drugs.

Electroporation uses electrical pulses to induce pore formation, which then may facility diffusion of drugs. Rapidly freezing and thawing exosomes is hypothesized to slightly disrupt the exosomal membrane.

#### 1.6.3.2 Exosome Surface Modifications

Although exosomes do intrinsically possess surface features that may confer specific targeting or binding activity, there may be interest to modulate or change these features by the use of engineered surface features. There are several ways to achieve this.

One method to modify the surface ligands is by use of genetic engineering. Cells are transfected with the vector gene of interest. Then, exosome produced by the transfected cells will express the gene, which may be displayed on the surface of the exosome.[54] Genetic engineering techniques are however, limited to only proteins that can be expressed. Moreover, these proteins must be transmembrane proteins or fused with a transmembrane protein. In addition, there is possibility that the genetically engineered protein will be expressed on the inner surface of the exosome,[104] thus requiring validation of external surface expression.

Chemical modification is an alternative strategy to modify exosome surfaces and can be divided into using non-covalent or covalent interactions. Non-covalent chemical modification commonly involves interaction the lipophilic membrane.[104] Interaction with the membrane is the mechanism of action for lipophilic membrane dyes such as the PKH dye series, but can also be used for polymer-lipid conjugates.[104] Chemical modification using covalent interactions are arguably superior to those using non-covalent interactions, as the probability that the interaction is disrupted is lower.[104] Click chemistry is used to refer to highly efficient, simple, reactions that can be used with biocompatible solvents or chemicals, and are commonly used in biotechnology to conjugate biomolecules. Classically, the 1,3-dipolar cycloadditions between azides and terminal alkynes is thought of as the cream of the crop of click chemistry reactions, due to its ease of use.[105] Click chemistry has been established for efficient conjugation of ligands to exosomes.[53,106] Exposed amine groups on proteins and lipids on the exosome surface can be functionalized

with cyclo-alkyne groups such as dibenzocyclooctyne (DBCO), using reactive N-hydroxysuccinimide (NHS) esters, while ligands can be functionalized with azide groups. Conjugation of ligand to exosome can then proceed efficiently through reactions between DBCO and azide groups.

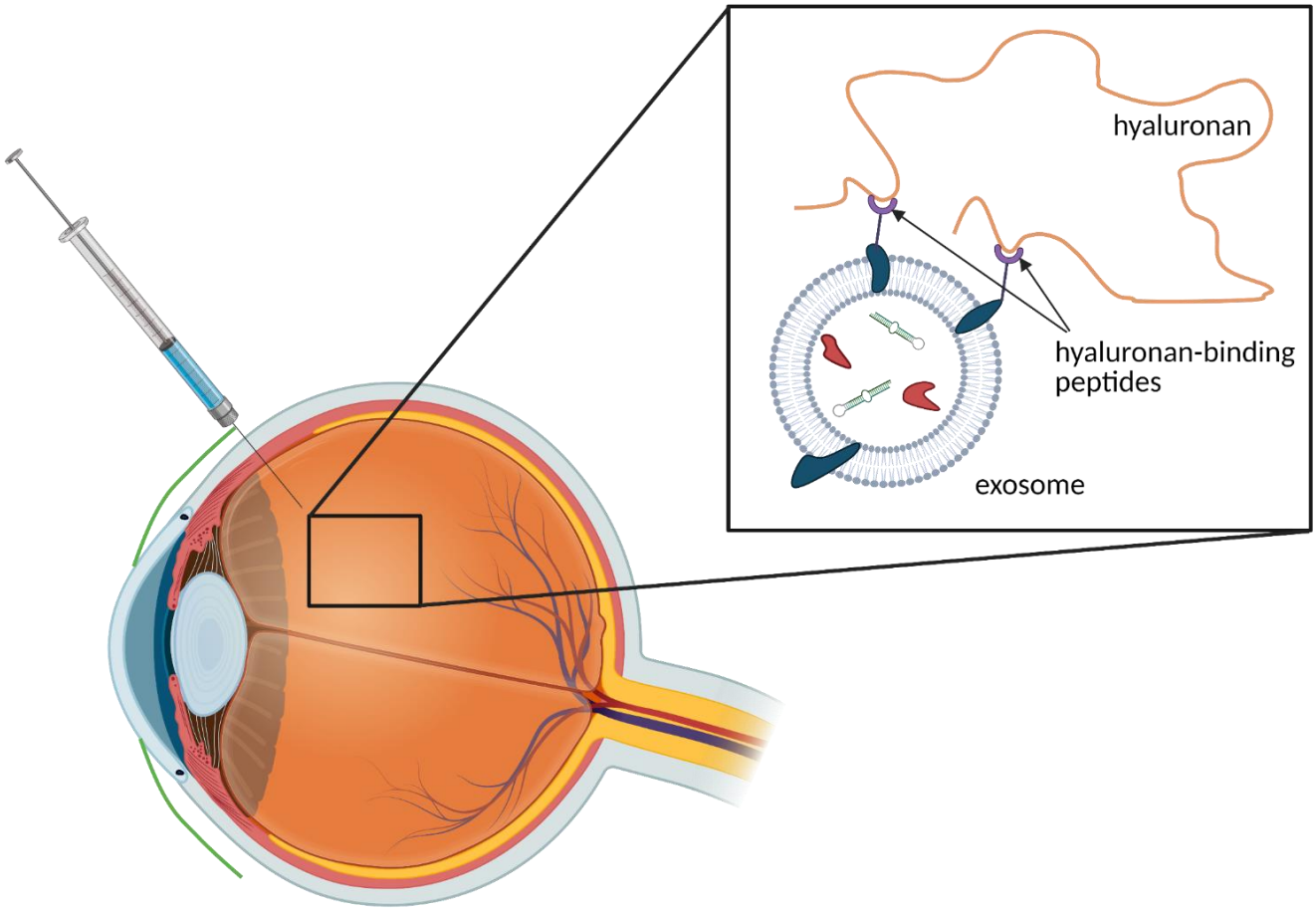


Figure 3. Schematic of the proposed drug delivery system. Exosomes are conjugated with HA-binding peptides to restrict diffusion in the VH and decrease clearance. The exosome suspension is injected intravitreally. Created with BioRender.com.

### 1.7 Rationale

Ocular anatomy and ocular pharmacokinetics present as a serious challenge, limiting the scope and effectiveness of pharmacotherapies that can be applied to posterior ocular diseases, such as in DR. It follows that the gold-standards for pharmacotherapy are the anti-VEGF agents, with wide therapeutic indices and relatively long half-lives due to their size. There are improvements that need to be made in drug delivery systems to allow for the delivery and evaluation of other drugs which have less favourable

properties. Namely, the system should aim to reduce injection frequency by exhibiting prolonged delivery after intravitreal injection, have biocompatibility, and protect any drug cargo from rapid degradation.

Exosomes are a novel class of drug delivery nanoparticles that have drug loading properties and biocompatibility, but a limited understanding of how they might function as drug carriers for the eye. To improve intravitreal retention time, use of in-silico designed HA-binding structures is a novel strategy. The use of exosomes conjugated with these peptides can potentially overcome several of the previously mentioned obstacles and function as a versatile system for effective intravitreal drug delivery.

## 1.8 Hypothesis

We hypothesize that HA-binding peptides can be intelligently designed using in-silico techniques and conjugated to exosomes to reduce the diffusion of exosomes in fluids containing HA.

## 1.9 Research Objectives

Aim 1: To isolate and characterize exosomes from ARPE19 cell culture.

Aim 2: To design and identity HA-binding peptides in-silico.

Aim 3: To evaluate the effectiveness of the peptides to reduce diffusion of exosomes in fluids containing HA.

# Chapter 2: Materials and Methods

## 2.1 Materials

Analytical grade water (CAWX0008-1) was purchased from VWR. ARPE19 cells (CRL-2302™) were purchased from ATCC. DMEM:F12 (319-085-CL), PBS (311-013-CL), trypsin-ethylenediaminetetraacetic acid 0.05% (325-042-CL), and penicillin-streptomycin solution 10,000IU (450-201-EL) were purchased from Wisent Bioproducts. FBS (26140095), exosome-depleted FBS (A2720801), Exosome Spin Column MW 3000 (4484449), dexamethasone-fluorescein (D1383) were purchased from ThermoFisher Scientific. 0.22 µm polyethersulfone syringe filters (SLGP033RB) and 100 kDa centrifugal filter units (UFC910024) were purchased from Millipore. MagCapture™ Exosome Isolation Kit PS (293-77601) was purchased from Fujifilm. CD63 protein (11271-H08H), monoclonal mouse anti-CD63 antibody (11271-MM10), and anti-mouse secondary antibody (SSA007) were purchased from SinoBiological. 3,3′,5,5′-Tetramethylbenzidine (TMB) ELISA substrate (ab171524), stop solution for TMB Substrate (ab171529), and ELISA wash buffer (ab172375) were purchased from Abcam. Glutaraldehyde (G151-1), acetonitrile (A998SK-4), and sodium hydroxide (10N; SS255) were purchased from Fisher Chemicals. UranyLess stain for electron microscopy (22409) and 200-mesh formvar-carbon coated grids (FCF200CU) were purchased from Electron Microscopy Sciences. Ethanol (362808), potassium dihydrogen phosphate (P5379), PKH26 labeling kit (MINI26), 4′,6-diamidino-2-phenylindole (DAPI), dexamethasone sodium phosphate (DSP) (PHR1768), fluorescein (F6377), coumarin-6 (442631) DBCO-sulfo-NHS ester (762040), Azido-dPEG®8-NHS ester (QBD10503), HA (molecular weight 1.5-1.8 million Da) (53747), and cetrimonium bromide (CTAB) (H9151) were purchased from Sigma Aldrich. Peptides were obtained from Genscript at 95% purity, with acetate anion. Sulfo-cyanine3 azide (A1330) was purchased from Lumiprobe. 0.2 µm membrane filters (66234) were purchased from Pall Corporation. 0.1 µm membrane filters (WHA800309) were purchased from Whatman.

## 2.2 Culture of ARPE19 Cells

Frozen ARPE19 cells were thawed in a 37°C water bath. Freezing medium was replaced with cell culture media containing DMEM:F12 supplemented with 10% FBS and 1% penicillin-streptomycin solution. The cells were incubated at 37°C with 5% $CO_2$ and passaged at 70-80% confluence. To passage, media was aspirated and followed by washing with PBS. To detach the cells, trypsin-ethylenediaminetetraacetic acid was added and the flask was incubated at 37°C for 15 mins. After incubation, the cells were observed under an inverted light microscope to ensure that all cells were detached. A large amount cell culture media was added to deactivate trypsin. The cell suspension was centrifuged at 125 rcf for 5 mins at room temperature to pellet the cells. The supernatant was aspirated, and the cell pellet was resuspended in media and seeded into an appropriate flask. Cells were subcultured to passage 30 before replacement. To produce environment for harvesting exosomes, the cells were seeded with cell media supplemented with 10% exosome-depleted FBS instead of FBS.

## 2.3 Exosome Isolation

The cells were cultured at 37°C until 80-90% confluent, at which point the cell culture supernatant was removed and sequentially centrifuged at 200 rcf and 2000 rcf, for 10 mins and 10000 rcf for 30 mins to remove cells, debris and microvesicles, respectively in the pellets. The resulting supernatant was filtered through 0.22 µm syringe filters to further remove larger particles. The clarified cell media was then concentrated to usable volumes (0.5 – 3 mL) using 100 kDa centrifugal filter units. Exosomes were isolated with magnetic beads according to the manufacturer's instructions or with UC twice at 150000 rcf for 2 hrs at 4°C in an MLS50 rotor (Beckman Coulter). Exosomes were stored at -20°C in PBS.

## 2.4 Exosome Characterization

### 2.4.1 CD63 ELISA

Exosome samples were characterized for presence of CD63 using indirect ELISA. CD63 in PBS was coated to wells of a 96-well ELISA plate by incubation at 4°C overnight. The solution was removed

and washed 3x with 100 µL wash buffer by flicking the plate over a sink. The remaining drops were removed by patting the plate on a paper towel. The remaining protein-binding sites were blocked by addition of 100 µL blocking buffer (1% bovine serum albumin in PBS), incubated for 2 hrs at room temperature, and the plate was washed 3x. Next, 100 µL of primary antibody (1:1000 in PBS) was added to each well, and the plate was covered with an adhesive plastic and incubated at 4°C overnight. Following 3x washing, 100 µL of secondary antibody (0.1 µg/mL in PBS) was added and the plate was covered with an adhesive plastic and incubated for 2 hrs at room temperature. Following 5x washing, detection was achieved by incubation with 100 µL TMB ELISA substrate for 10 mins at room temperature. Then, 100 µL stop solution was added to each well to stop the reaction and absorbance was measured at 450 nm.

### 2.4.2 Biophysical

Exosomes samples were characterized for size distribution and concentration using NTA (Nanosight LM300). Samples were diluted with PBS if necessary to achieve the particle concentration recommended by the manufacturer. Five recording of 60s each were made for each measurement, and the syringe pump was used whenever possible. The instrument was set to a camera level of 16, detection threshold of 5, room temperature, and the other settings were left on default. NTA was used frequently before and certain experiments to validate the protocol or ensure morphology had not significantly changed.

Zeta potential was evaluated using DLS (Zetasizer Nano ZS). The zeta potential of exosome samples diluted in water was measured in DTS1070 cuvettes (Malvern Panalytical) in a Zetasizer Nano ZS (Malvern Panalytical) by making five recordings of 60s each at 25°C.

### 2.4.3 Morphology

Exosome morphology was characterized by scanning TEM (STEM) or TEM. The exosome sample was fixed by incubation in glutaraldehyde (2.5% v/v) in PBS, overnight at 4°C. Then, 10 µL of the fixed sample was pipetted into a drop onto a clean piece of parafilm. Next, the formvar-carbon coated copper

grid was gently placed with the rough side in contact with the drop and left to adhere to the sample for 30 mins at room temperature. Then, the grid was dried by touching the smooth side to filter paper. Next, a 10 µL drop of UranyLess stain was pipetted onto a clean piece of parafilm. The grid was then added with rough side in contact with the drop and left to adhere to the sample for 1 minute. The grid was dried again using filter paper and then dried using a vacuum pump overnight. The sample was imaged by TEM (ZEISS LIBRA® 200 MC) at 200 kV, or by STEM (ZEISS ULTRA plus) at 20 kV.

### 2.5 Exosome Cell Uptake

The exosome suspension was labeled by mixing with 6 µM PKH26 in Diluent C in a 1:1 ratio, followed by 15 mins of incubation at room temperature. Then, 100 µL labeled exosomes were passed through exosome spin columns according to the manufacturer's instructions, and the eluate was collected. Dye solution without exosomes was used as a control group for this step. ARPE19 cells were seeded at a density of 10000 cells/well in 96 well tissue culture plates and given 24 hrs to attach. 75 µL eluate was mixed with 525 µL media, and 200 µL of the mixture was added to each well.

At specified timepoints (3, 12, and 24 hrs), the media was removed and cells were washed with PBS. Then, cells were labeled with 10 µg/mL DAPI by incubation at 37°C for 20 mins. Cells were washed with PBS and imaged immediately in PBS under microscopy (EVOS FL Auto) using the phase contrast, DAPI, and red fluorescent protein (RFP) modules.

### 2.6 Drug Loading

Detection of DSP was performed using ultra-performance liquid chromatography (UPLC). Chromatographic separation was performed on a ACQUITY UPLC HSS C18 Column (100Å, 1.8 µm, 2.1 mm X 100 mm; Waters, MA, USA) fitted to a Waters® Alliance® UPLC. Detection was performed with a tunable UV-Visible detector working at 240 nm. The concentration of DSP was determined using isocratic elution with 67.5% acetonitrile, 32.5% 0.01 M potassium dihydrogen phosphate in water as mobile phase. The total run was 2 min for each 5 µL injection, with a flow rate of 0.5 mL/min at room

temperature. DSP of known concentrations (5-100 µg/mL) was used to generate calibration curves. Calibration curves were checked for linearity (R2). Unknowns were quantitated using area under the curve. Fluorescein was quantitated by creation of a calibration curve (0.1 – 1000 ng/mL) and fluorescence measurements (excitation: 488 nm, emission: 525 nm). Coumarin-6 was quantitated by creation of a calibration curve (0.1 – 1000 ng/mL) and fluorescence measurements (excitation: 488 nm, emission: 525 nm).

For drug loading experiments, UC was used to separate exosomes from excess drug. In certain cases, encapsulation efficiency (EE) was calculated indirectly by measurements of the supernatant using the following equation:

$$Encapsulation\ Efficiency\ (\%) = \frac{Amount\ initial\ drug - Amount\ unencapsulated\ drug\ (supernatant)}{Amount\ initial\ drug} \times 100\%$$

In other cases, EE was calculated directly by measurements of drug in the pellet using the following equation:

$$Encapsulation\ Efficiency\ (\%) = \frac{Amount\ encapsulated\ drug\ (pellet)}{Amount\ initial\ drug} \times 100\%$$

### 2.6.1 Sonication Method

For the sonication method, exosomes (~$10^{10}$ particles/mL) and model drug (DSP: 25 µg/mL, fluorescein: 1 µg/mL, coumarin-6: 1 µg/mL) were sonicated on ice for 30s on/off for 3 mins per cycle for 3 cycles with 1 minute between cycles at amplitude 5 using an ultrasonicator (Qsonica S-4000). The sonicated sample was rested for 30 mins at 37°C to allow for exosomal membrane recovery. UC was used 2x to wash exosomes from excess drug. The supernatant of the first UC was recovered to quantify excess drug.

### 2.6.2 Cell Culture Incubation Method

DSP (100 or 1000 µg per 75cm$^2$ flask) was added to ARPE19 cells at ~50% confluency and given 48 hrs to incubate. Exosomes were then isolated by the UC method mentioned in Section 2.2. The pellet was resuspended in 1 mL mobile phase to lyse the exosomes and release the drug for quantitation.

## 2.7 Molecular Docking

All molecular docking studies were conducted using Discovery Studio, *Structure-Based-Design* software (BIOVIA Inc. San Diego, USA). During the computational studies, anionic polymer HA was set as the receptor and a library of linear peptides were designed and used as ligands for HA. The x-ray structure of HA was obtained from Protein Data Bank (PDB id: 2JCQ).[44] This model obtained represents a complex of binding domain of murine CD44 with HA 8-mer. The HA receptor was prepared after deleting CD44 and water using CHARMm force field. The crystal structure of HA fragment, was an octomer with 8-sugar units. However, the electron density of one of the sugar units was not visible. Therefore, the crystal structure of HA was modified and was extended further by adding five more sugar units with alternating disaccharide D-glucuronic acid and N-acetyl-D-glucosamine units linked together to obtain a 12-mer HA by manually adding five extra units to the original x-ray structure (Figure 4). Then, the HA 12-mer model was subjected to energy minimization by using steepest descent followed by conjugate gradient minimization (1000 steps each) using a distance dependent dielectric constant and CHARMm force field. This model was then used to conduct molecular docking studies. A receptor binding sphere of 32 Å radius which covers the entire 12-mer HA was used to dock the peptides. The peptide library was built in *small molecule* module and subjected to energy minimization via both steepest descent and conjugate descent minimization using CHARMm force field. Then, the docking was carried out using the *receptor-ligand interactions* module in Discovery Studio. The CDOCKER algorithm was used for docking studies. This algorithm uses a molecular dynamics based simulated annealing protocol to identify ligand binding poses.[107] The binding modes obtained were ranked according to CDOCKER

and CDOCKER interactions energies for CDOCKER algorithm, to identify top ranked poses of peptides with HA. Intermolecular polar and nonpolar interactions were analyzed to understand the interactions of peptides with HA.[108]

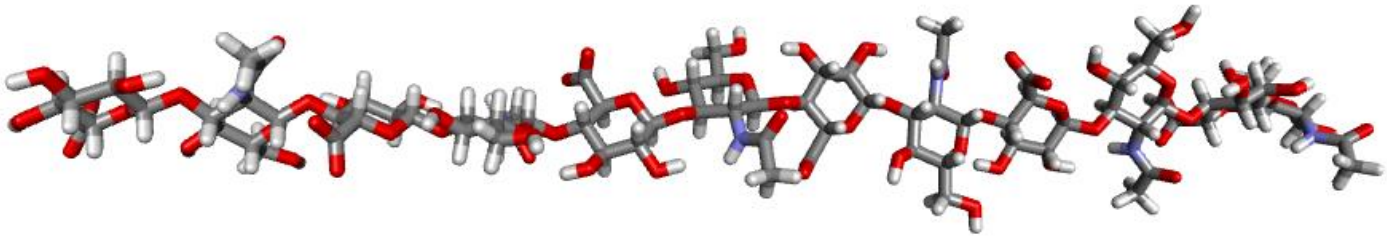

Figure 4. Structure of 12-mer long HA built using the modeling software Discovery Studio.

## 2.8 Modification of Exosome Surface

Exosomes ($2.75x10^{11}$ particles/mL) were incubated with 50 µg/mL DBCO-sulfo-NHS ester in 1 mL PBS for 4 hrs at room temperature under rotation to functionalize the exosomes with DBCO groups. Control groups without exosomes or without DBCO-sulfo-NHS ester were also evaluated. DBCO-exosomes were washed with PBS twice using UC and resuspended in ~0.5 mL PBS.

For validation of the chemical conjugation, functionalized exosomes were incubated with ~1 µM sulfo-cyanine3 azide overnight at 4°C to conjugate cyanine3 (Cy3) onto the exosomes. Conjugated exosomes were washed with PBS twice using UC and resuspended in ~0.5 mL PBS. Light-mode NTA was used to evaluate exosome recovery efficiency. Fluorescent (532 nm laser module, 569 nm filter) NTA was used to evaluate the fraction of exosomes that were fluorescent as a measure of labeling efficiency. A fluorescence plate reader (532 nm excitation, 570 nm emission) and creation of a calibration curve for sulfo-Cy3-azide was used to estimate fluorophore recovery efficiency.

Peptides were functionalized with Azido-dPEG®8-NHS ester in 9x molar excess by incubation at room temperature for 4 hrs. For conjugation with peptide, sulfo-Cy3-azide was replaced with azide-functionalized peptide in the same protocol.

## 2.9 Evaluating the Effect of Peptide Conjugation on Diffusion Rate in HA

To evaluate the effect of peptide conjugation on exosome diffusion rate, a diffusion cell model was created. HA was slowly dissolved at 1 mg/mL in PBS at 37°C. To validate the model and membrane filters for potential HA leakage, a Franz diffusion cell (PermeGear) was used. The experiment was setup with 1 mL HA solution (1 mg/mL) in the donor chamber of the diffusion cell, 5 mL PBS in the receptor chamber, the bath temperature was set to 34°C to mimic the temperature of the eye, and filter membranes with either 0.1 or 0.2 µm pore sizes. At specified timepoints (1, 2, 4, 8, and 24 hrs) the receptor chamber was sampled and replaced with an equal volume of PBS to maintain chamber volume.

HA concentration was measured using a modified HA quantification test.[109] Briefly, HA solution or test samples were heated to and kept at 37°C until needed. CTAB was prepared at 25 mg/mL in 0.5 M sodium hydroxide solution and kept at 37°C until needed. CTAB solution was aliquoted to each well of a 96 well plate. An equal volume of HA standard (0 - 250 µg/mL) or test sample was added to wells containing CTAB, and absorbance at 600 nm was immediately measured. Data was expressed as a percent diffusion, based on the initial HA in the donor chamber. To account for the sampling volume, cumulative concentration was calculated using the following equation:

$$Cumulative\ concentration\ at\ time\ t = \frac{volume\ sampled\ (mL)}{total\ bath\ volume\ (mL)} \times C(t-1) + C(t)$$

$$Where\ C(t)\ =\ concentration\ measured\ at\ current\ timepoint$$

$$Where\ C(t-1)\ =\ concentration\ measured\ at\ previous\ timepoint$$

To evaluate exosome or model drug diffusion, the diffusion cell was setup with 1 mL HA solution (1 mg/mL) in the donor chamber, 5 mL PBS in the receptor chamber, 0.1 µm membrane filter, and the temperature set to 34°C. Peptide-modified exosomes or control exosomes were fluorescently labeled with PKH26 by incubation for 15 mins at room temperature in 6 µM PKH26 in Diluent C. Excess dye was removed by UC, and the labeled exosomes were resuspended in HA solution and tested for initial

fluorescence. As a relevant small-molecule model drug, dexamethasone-fluorescein was prepared at 10 µg/mL in HA solution and tested for initial fluorescence.

The samples were then placed in the donor chamber. At specified timepoints (1, 2, 4, 8, and 24 hrs), the receptor chamber was sampled and replaced with an equal volume of PBS. To measure PKH26 concentration, samples were diluted to 50/50 (v/v) ethanol/PBS, tested for fluorescence using a plate reader (510 nm excitation, 570 nm emission), and quantitated using a calibration curve. To measure dexamethasone-fluorescein concentration, samples were tested for fluorescence using a plate reader (488 nm excitation, 525 nm emission), and quantitated using a calibration curve.

Data was expressed as a percent diffusion, based on the initial fluorescence in the donor chamber. To account for the sampling volume, cumulative concentration was calculated using the previously stated equation.

# Chapter 3: Results and Discussion

## 3.1 Exosome Isolation and Characterization

### 3.1.1 CD63 ELISA

Checkerboard titration (Table 1) was used to optimize the concentration of the ligand and primary antibody. The secondary antibody was fixed at a concentration of 0.1 µg/mL as recommended by the manufacturer. Based on the checkerboard titration, a maximum concentration of 32 ng/mL of antigen and 1:1000 concentration of primary antibody was determined for use in future tests. Next, a calibration curve (n = 3) was produced to determine the linearity and reliability of the assay (Figure 5).

Table 1. Checkboard titration absorbance values at 450 nm of the antigen and primary antibody for CD63 ELISA. The secondary antibody was used at a concentration of 0.1 µg/mL as recommended by the manufacturer. Values are displayed up to two decimal digits.

| **Absorbance at 450 nm** | | **Antigen concentration (ng/mL)** | | | | | | | | | |
|---|---|---|---|---|---|---|---|---|---|---|---|
| | | **100** | **50** | **25** | **12.5** | **6.25** | **3.125** | **1.56** | **0.78** | **0.39** | **0** |
| **Primary antibody dilution** | **1 in 500** | 3.17 | 3.11 | 2.99 | 2.79 | 2.72 | 2.48 | 1.95 | 1.34 | 0.93 | 0.13 |
| | **1 in 1000** | 2.9 | 2.96 | 2.92 | 2.84 | 2.57 | 2.37 | 1.66 | 1.31 | 0.7 | 0.08 |
| | **1 in 2000** | 2.84 | 2.66 | 2.79 | 2.46 | 2.28 | 2.05 | 1.41 | 0.92 | 0.71 | 0.10 |

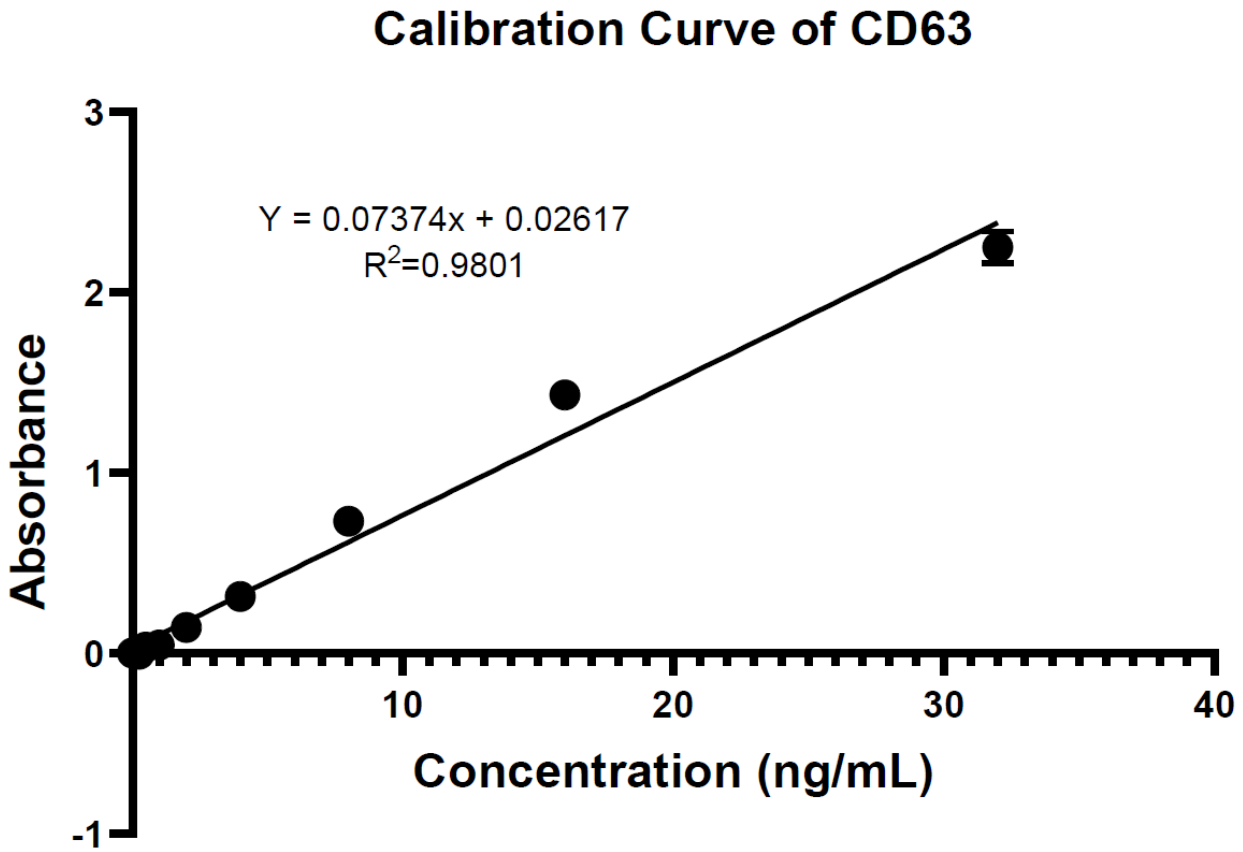


Figure 5. ELISA calibration curve of CD63. Known concentrations of CD63 (0 – 32 ng/mL) were used. Absorbance was measured at 450 nm. Linear regression was used to generate a calibration curve. Values were normalized by the blank average. Values represent mean ± SD (n = 3).

Exosomes from bead-based isolation method were relatively high in CD63 content, producing between 116 ng of detectable CD63 per ~50 mL cell culture fluid. On the other hand, exosomes from UC isolation method were comparatively low in CD63 content, producing 15.5 ng of detectable CD63 per ~50 mL cell culture fluid.

According to these results, it is possible the Tim4 bead-based isolation method produced exosomes of higher purity, given that CD63 is a marker for exosome enrichment. These results are supported by findings of others that the Tim4 bead-based isolation isolated approximately 10x more exosomal RNAs compared to UC.[110] This is expected as the Tim4 bead-based isolation method is based on affinity between Tim4 and phosphatidylserine, which is displayed on exosomal surfaces.[110]

However, there are alternative explanations as well. The Tim4 bead-based isolation is claimed by the authors' to be superior to other antibody-based affinity capture methods as the exosomes are detached

from the beads without lysing the exosomes.[110] However, there was no information on how lysis rates might compare between Tim4 bead-based isolation and UC.

Due to the bead-based isolation method requiring chemical-based disassociation of exosomes from the bead, it is possible that this process, when compared to UC, resulted in increased lysis of the exosomes and release of CD63 into solution. Furthermore, the validity of our CD63 ELISA was limited as only tested using free floating CD63, and it is possible that CD63 in free-floating form might have completely different coating properties to CD63 found in exosomes. Since, there is no information in the literature regarding how exosomes might interact with an ELISA plate during the coating process. Since ELISA coating is mostly defined and validated for coating of proteins, it is possible that the intact exosomes (in colloidal form) decreased the coating efficiency of any transmembrane CD63 on the exosomes. A possible solution to the exosome protein coating issue can be to use a lysis buffer (e.g. RIPA buffer) to ensure all exosomes are lysed prior to coating.

### 3.1.2 Size Distribution, Zeta Potential, Morphology, and Yield

Exosomes isolated by affinity capture from ARPE19 cell culture had a diameter of 100.8 ± 27.2 nm as measured by NTA (Figure 6A). Approximately $10^{10}$ exosomes could be isolated from 100 mL cell culture fluid. Exosomes had spherical morphology as determined by TEM (Figure 6B). TEM revealed presence of smaller spherical particles that could not be detected using NTA. The stated detection limit of NTA (10 nm), is affected by the scattering properties of the particle. As exosomes are weakly scattering particles, a higher detection limit is expected, and explain why NTA could not detect the smaller particles observed by TEM. Based on approximate size and morphology, the identity of these smaller particles (<30 nm) is likely to be lipoproteins, which can range from 10 – 40 nm depending on lipoprotein class. Lipoproteins are major component of FBS that is used in cell culture, and thus are commonly co-isolated with exosomes. Interestingly, lipoproteins are co-isolated with exosomes using the Tim4 bead-based isolation method. Tim4 beads should not have affinity to lipoproteins as lipoproteins do not contain

phosphatidylserine.[111] This, along with the finding that many isolation methods co-isolate lipoproteins, could suggest that lipoproteins have affinity to exosomes.

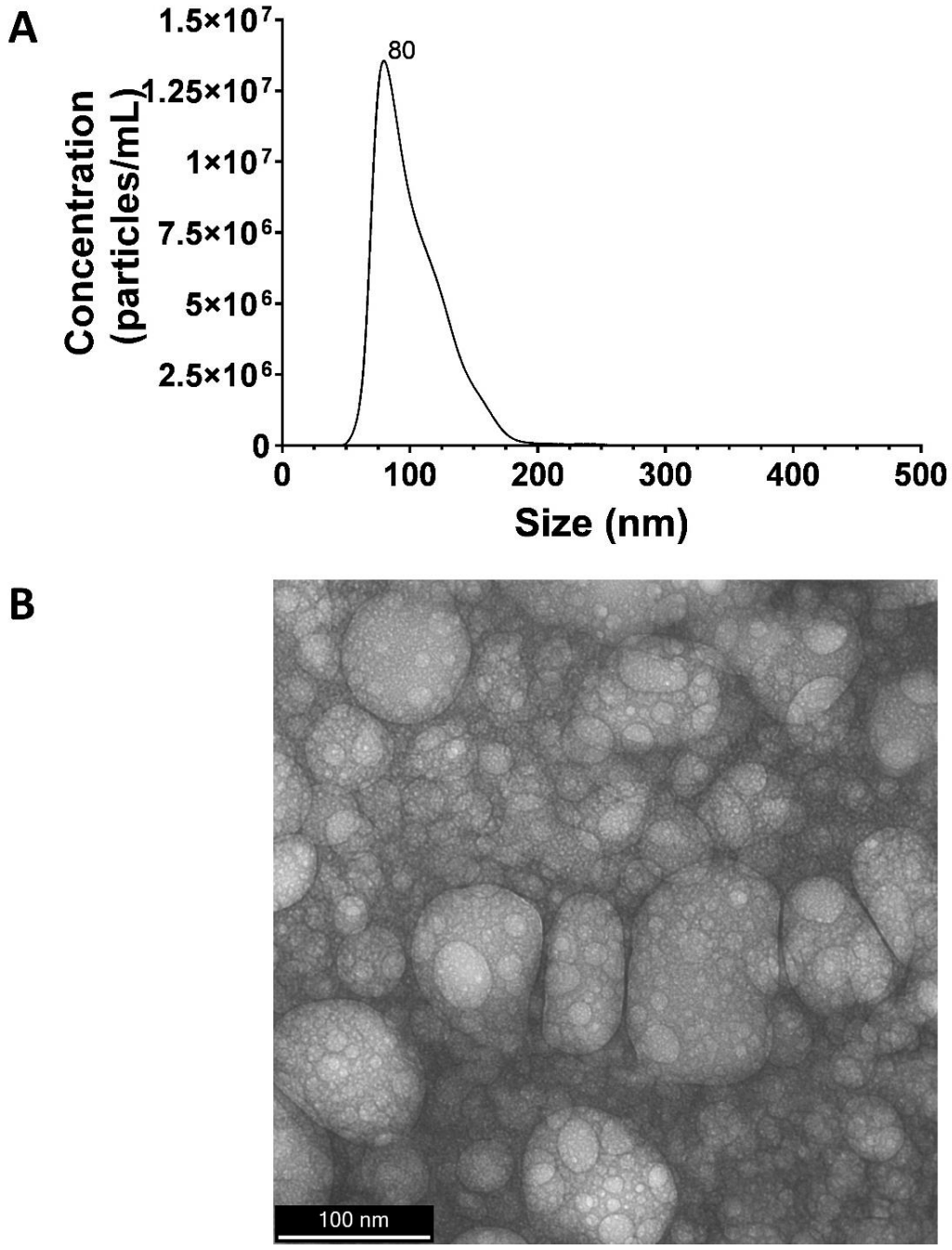


Figure 6. (A) Size distribution of exosomes isolated by MagCapture™ Exosome Isolation Kit PS as measured by NTA and (B) TEM image. The magnification used was 40x for NTA and 50000x for TEM.

Exosomes isolated by UC from ARPE19 cell culture had a mean diameter of 85.0 nm (Figure 7A). Exosomes isolated by UC had a mean zeta potential of -16.32 ± 2.44 mV. Approximately $10^{12}$ exosomes could be isolated from 100 mL cell culture fluid. Exosomes had spherical morphology as imaged by STEM (Figure 7B). Interestingly, both NTA and STEM were able to detect smaller particles in the 20 nm range. The NTA results might indicate that UC co-isolates a higher fraction of lipoproteins than the Tim4 bead-based isolation method. As a result of sample containing a higher of lipoproteins, the overall increase scattering intensity from these lipoproteins might manifest itself as a peak that could be detected by NTA. Given that UC is also a method commonly used to isolate lipoproteins,[111] it is highly likely that lipoproteins will co-isolate with exosomes while using UC.

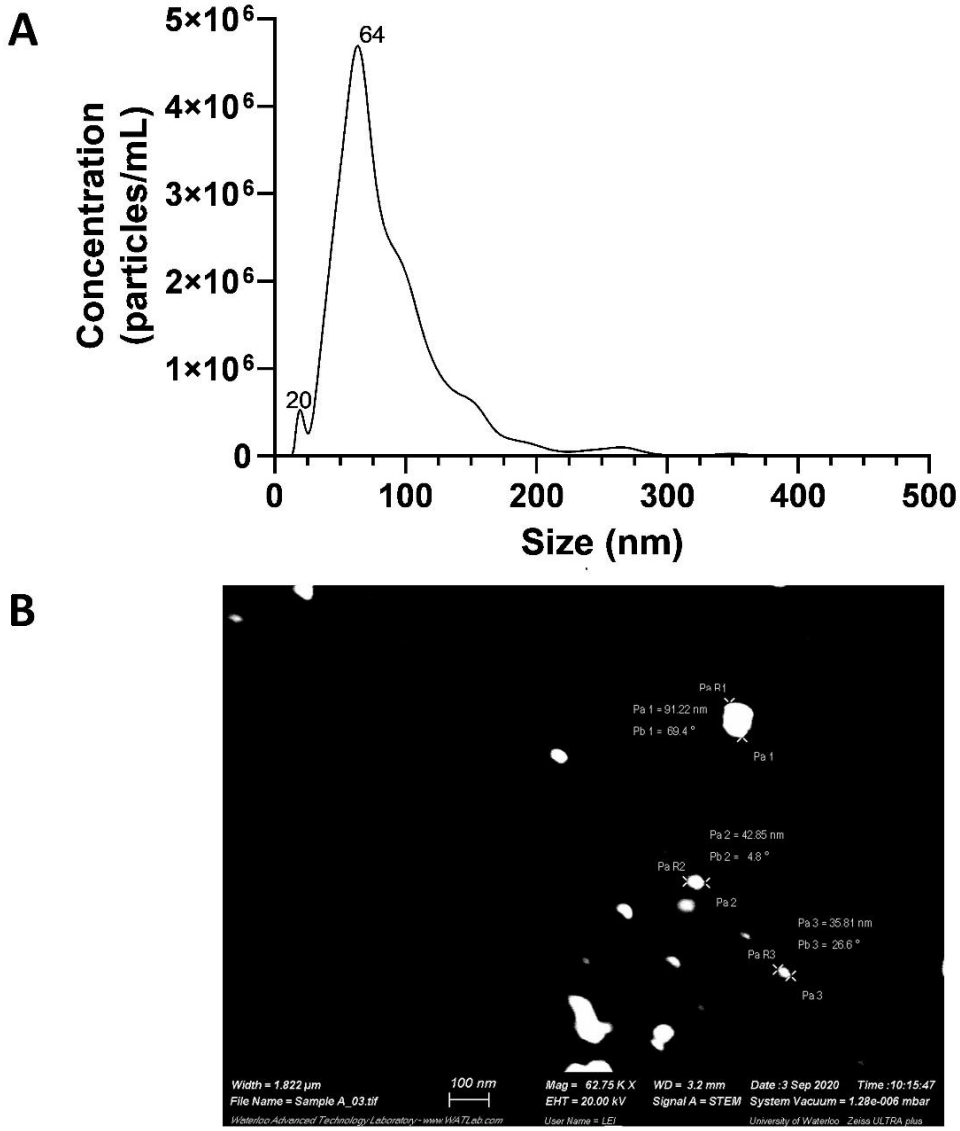


Figure 7. (A) Size distribution of exosomes isolated by UC as measured by NTA and (B) STEM image. The magnification used was 40x for NTA and 627500x for STEM. Three particles of varying diameters are estimated on the STEM image.

Given that lipoproteins also can be used to mediate drug delivery, it is important to aim to have a lipoprotein-free isolation process.[63] Unfortunately, there are not many effective strategies to avoid co-isolation of lipoproteins with exosomes while maintaining other good isolation properties.[103] This is due to lipoproteins and exosomes having similar overlapping biophysical characteristics. If FBS (containing lipoproteins) is necessary for cell culture growth, it would be recommended to quantitate the amount of lipoproteins in the isolate by means of ELISA or Western Blot.[103] Alternatively, if use of FBS can be

avoided, the possibility of lipoprotein contamination can be avoided, but this is not possible for all cell lines.[103]

Nevertheless, there is still discussion surrounding the optimal isolation and characterization methods. Currently, the most used isolation methods are not perfectly optimized. As such, there exists tradeoffs for various isolation methods between yield, purity, ease of use, and other factors.[103] Development of new methods or protocols is likely necessary to further improve our ability to conduct exosome research.

UC, being the first, most well established, and simple method, along with our data showing that it produced isolates appearing to have mostly exosome-sized particles along with good particle yield. Even if bead-based isolation can produce better exosome enrichment, exosome enrichment is not the be-all and end-all for selection of a method especially for drug delivery, as other factors are also important.[103] Importantly, yield and ease of use were two contributing factors to the decision to eventually use UC as the primary isolation method.

### 3.2 Exosome Cell Uptake into ARPE19 Cells

ARPE19 cells exhibited the expected morphology and size (~20 μm) as reported in literature.[112] PKH26-labeled exosomes qualitatively displayed time dependent uptake into ARPE19 cells as seen in Figure 8. At 3 hrs, there was little cell uptake. At 12 and 24 hrs, there appeared to be a high level of cell uptake. The control group (dye solution without exosomes in spin column) displayed no evidence of cell uptake. Cells at different timepoints appeared to show differing intensities of DAPI staining.

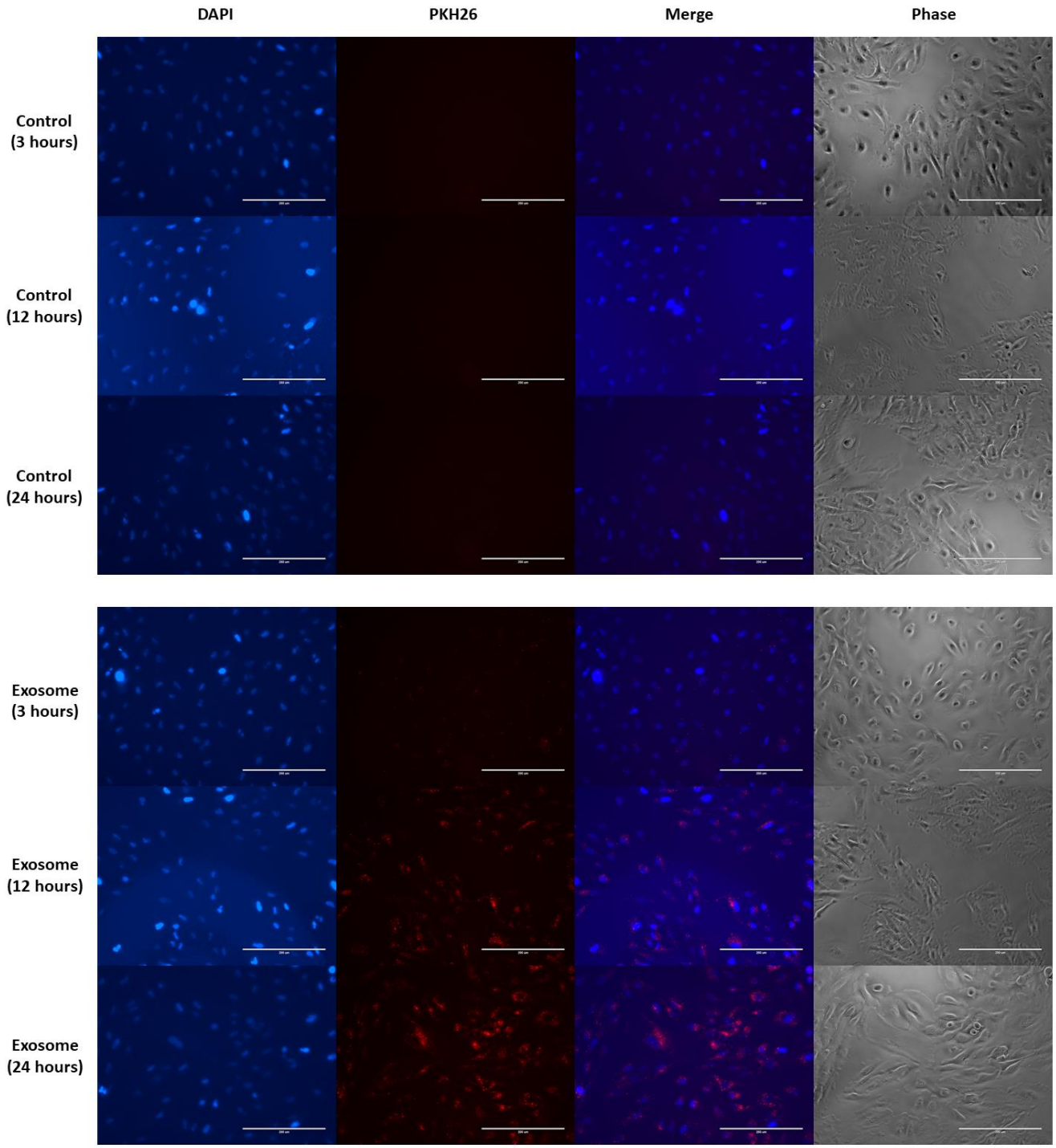


Figure 8. PKH26-stained exosomes displayed time dependent uptake into ARPE19 cells. At 3 hrs, there was little cell uptake. At 12 and 24 hrs, there appeared to be an increased level of cell uptake. The control group (dye solution without exosomes in spin column) displayed no evidence of cell uptake. The magnification was 20X and the scale bar represents 200 µm. In blue is DAPI and in red is PKH26.

It is interesting that DAPI staining intensity varied between the different timepoints. DAPI permeates the membrane to intercalate with nuclear deoxyribonucleic acid (DNA), and emit fluorescence

when excited.[113] DAPI staining intensity is affect by the amount of DNA in the cell and the permeability of the cell membrane.[113] In the absence of cell permeabilizer, live cells need to be stained with concentrations of DAPI (10 µg/mL) greater than the concentrations used for permeabilized cells (~1 µg/mL). If cells are in different stages of the cell cycle or in the process of dying, there might be different amount of DNA in the cells, permeabilities and thus differing DAPI staining. To ensure that all cells at all timepoints are permeabilized, cells can be fixated (commonly with formaldehyde) and then permeabilized with a detergent.[114]

Although the results indicate time-dependent uptake of exosomes into the cells, it does not fully elucidate the mechanism of uptake. Based on the images, PKH26 does not appear to be distributed among the cell membrane, and thus internalization is more likely than membrane-membrane fusion. A simple addition to this study could be to add PKH26 to cells as a positive control group for membrane-membrane fusion. The possible routes of exosome uptake into target cells include clathrin-dependent endocytosis, caveolae-dependent endocytosis and other mechanisms.[115,116] To elucidate the mechanism of uptake, inhibitors of the various uptake routes should be used along with quantitation using FC.

Exosome cell uptake is one modality that might facilitate drug entry into target cells. As the primary physiological function of exosomes are to mediate cell-cell communication through binding and/or transfer of biomolecules,[103] exosomes are expected to possess intrinsic cell uptake properties. In the context of this project, these results might suggest that if exosomes are able to diffuse to RPE cells in the retina, cellular uptake and delivery of cargo may be a mechanism to mediate therapeutic effect. Based on DR pathology, targeting other cells such as Müller cells or vascular endothelial cells might be important.[117] In addition, it is known that exosome-uptake into cells is recipient-cell dependent.[115] Thus, it would be useful to quantitate, using image analysis or FC, how exosomes from different cellular sources might have different uptake properties in different cell lines. Quantitation of these cell uptake parameters, in the future, might allow for design of a drug delivery system with better cell targeting.

### 3.3 Exosome Drug Loading

For the sonication method, EE was negligible in all cases. DSP EE (Table 2), as measured both directly and indirectly, was negligible. Negligible drug loading was obtained for both fluorescein and coumarin-6. For the pre-loading by incubation with cell culture method, EE was negligible as no drug could be detected in the pellets.

Table 2. Drug loading of DSP by sonication and calculation of EE indirectly and directly.

| **Calculation method** | | **EE (%)** | **SD (%)** |
|---|---|---|---|
| **Indirect (Supernatant)** | Experimental (n = 3) | -17.76 | 3.96 |
| | Control (n = 1) | -11.65 | N/A |
| **Direct (Pellet)** | Experimental (n = 3) | 0.81 | 0.24 |
| | Control (n = 1) | 1.05 | N/A |

A possible explanation for the negative EE observed (when EE was measured indirectly) is that during the sonication process, liquid evaporation might increase the drug concentration. When combined with negligible drug loading, this might result in negative EE values when making supernatant measurements.

DSP was initially selected as it is small molecule drug which is clinically used to treat several posterior ocular diseases, including diabetic macular edema, glaucoma, and DR.[12,118,119] Fluorescein and coumarin-6 were selected as hydrophilic and hydrophobic fluorescent model of small molecule drugs. Due to their fluorescent nature, these model drugs would have a lower detection limit, which was determined to be ~0.1 ng/mL which was several orders of magnitude lower than the detection range for DSP which was ~5 µg/mL. Thus, by using drugs with a lower detection limit, it will also allow for use of a lower concentration of drug, and the increased precision of detection might allow for detection of small

changes in drug concentrations. For example, if the drug loading procedure caused a very low amount of drug loading due to the loading capacity of the exosome being reached, where loading capacity is the maximum amount of drug that can be loaded per exosome, being able to use and detect lower concentrations might be useful in if low loading capacity is responsible for the observed results. Use of lower initial drug concentrations should also result in increased EE (if loading capacity is achieved), as EE is calculated based on the initial amount of drug used.

However, the poor EE of fluorescein indicate that it is unlikely that exosome loading capacity being reached is the sole factor for the poor drug encapsulation. Thus, increasing exosome concentration in relation to drug concentration, at this stage of optimization, is not suitable. There is a likelihood that several other factors related to sonication parameters or drug properties contribute to the poor EE.

Based on exosome structure, during drug loading processes, lipophilic drugs should distribute within the lipid bilayer while hydrophilic drug should distribute within the lumen.[103] PubChem estimated coumarin-6, fluorescein, and DSP to have LogP of 4.9, 3.4, and 1.9, respectively. LogP is a measure of hydrophobicity, where greater values indicate greater hydrophobicity. During drug loading, coumarin-6, would be expected to mostly distribute within the bilayer, while DSP comparatively would distribute more the lumen. Thus, it is likely exosomes have different loading capacities for drugs with different properties. Moreover, it is likely that different drug loading methods will be more suited to loading of drug of different properties. For example, use of a passive loading method where the membrane is not disturbed might be more suited to loading of lipophilic drugs that can permeate lipid membranes (e.g. exosome membrane), while being ineffective for loading of hydrophilic drugs which don't easily permeate lipid membranes. Thus, use of an active loading method that creates transient pores is likely necessary for loading of hydrophilic drugs. To improve drug loading, alternative drug loading strategies such as should be investigated such as electroporation, freeze-thaw cycling, extrusion, or use of permeabilizers.[103]

### 3.4 In Silico Design of HA Binding Peptides

The list of docked peptides is shown in Table 3 and the top ranking docking poses are shown in Figure 9 and Figure 10. Both short cationic and anionic cationic linear peptides failed to dock to HA and did not show any binding poses. Peptides designed based on the B-(X7)-B motif which contain amino acids arginine (R) and glycine (G) were able to bind to HA. Modifications to this motif such as repeat units, spacer length modification, and additional basic amino acids at the termini modified their HA binding properties.

Table 3. The names, length, sequence and docking results of HA binding of linear peptides. The docking poses were ranked using the CDOCKER energy values (ligand-receptor complex energy). Greater negative CDOCKER energy indicates greater peptide-HA complex stability.

| Name | Description | Length (AA) | Sequence | Docking Result | CDOCKER ENERGY in kcal/mol |
|---|---|---|---|---|---|
| **C2** | short cationic | 2 | RR | No poses | |
| **C3** | short cationic | 3 | RRR | No poses | |
| **C4** | short cationic | 4 | RRRR | No poses | |
| **C5** | short cationic | 5 | RRRRR | No poses | |
| **C9** | long cationic | 9 | RRRRRRRRR | Yes | -86.79 |
| **A5** | short anionic | 5 | DDDDD | No poses | |
| **Bx4B** | 4 spacers | 6 | RGGGGR | Yes | -73.14 |
| **Bx5B** | 5 spacers | 7 | RGGGGGR | Yes | -79.40 |
| **Bx6B** | 6 spacers | 8 | RGGGGGGR | Yes | -86.01 |
| **Bx8B** | 8 spacers | 10 | RGGGGGGGGR | Yes | -98.22 |
| **Ax7A** | anionic version | 9 | DGGGGGGGD | Yes | -86.53 |
| **Bx7B1** | 1 repeat | 9 | RGGGGGGGR | Yes | -95.51 |
| **Bx7B2** | 2 repeats | 17 | RGGGGGGGRGGGGGGR | Yes | -128.73 |
| **Bx7B3** | 3 repeats | 25 | RGGGGGGGRGGGGGGRGGGGGGGR | Yes | -194.95 |
| **BBx5BB** | double basic 5 spacer | 9 | RRGGGGGRR | Yes | -99.51 |
| **BBx6BB** | double basic 6 spacer | 10 | RRGGGGGGRR | Yes | -111.01 |

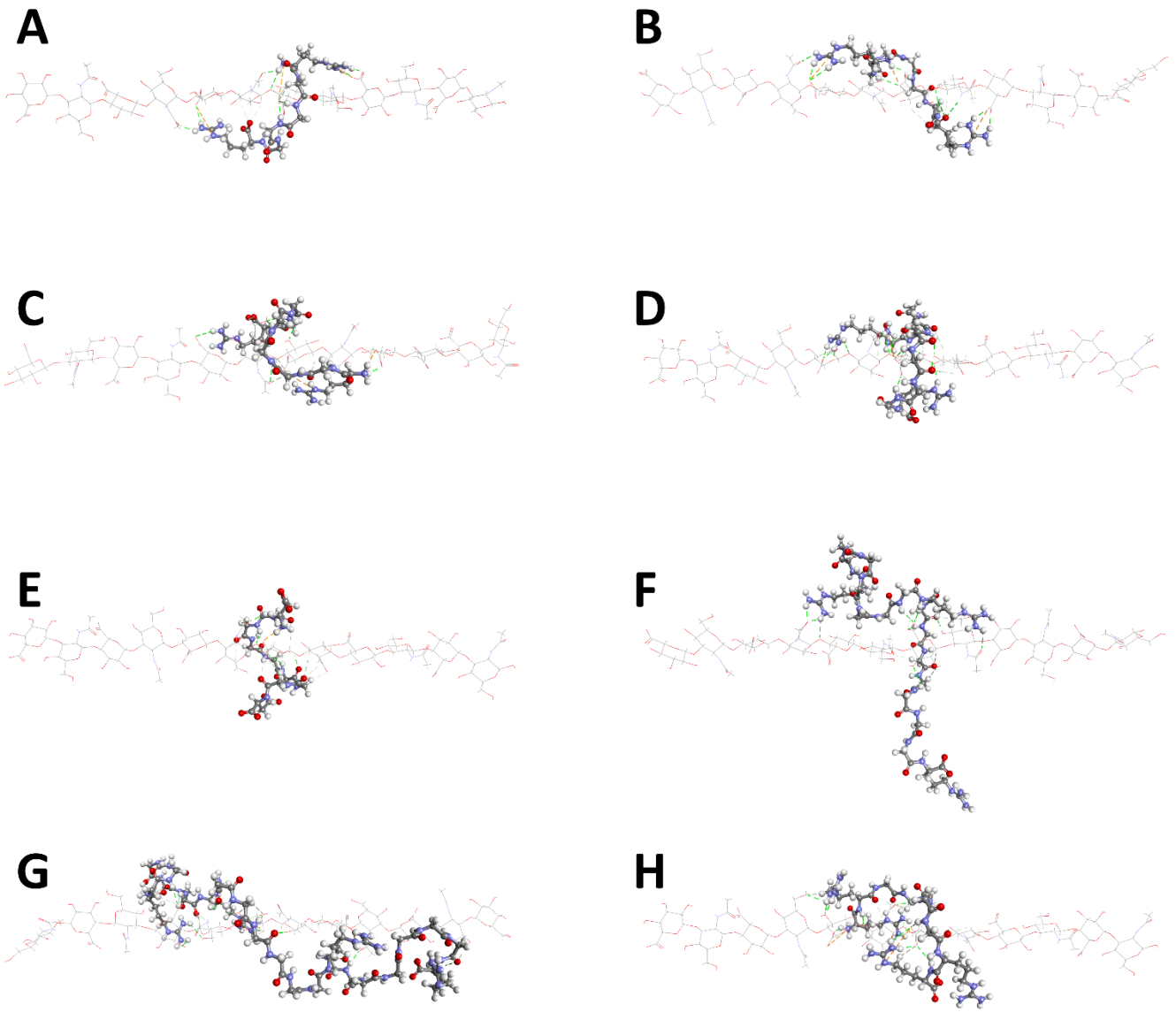


Figure 9. Predicted top ranking binding pose of peptides (ball and stick cartoon) to 12-mer HA. The top ranking binding poses of (A) Bx4B, (B) Bx5B, (C) Bx6B, (D) Bx8B, (E) Ax7A, (F) Bx7B2, (G) Bx7B3, and (H) BBx5BB are shown. Atoms of carbon, oxygen, nitrogen, and hydrogen (not displayed for HA) are displayed in grey, red, blue, and white, respectively. Intermolecular bonds between HA and peptides are displayed in green for hydrogen bond interactions and orange for electrostatic interactions. Lighter shaded interactions indicate the interaction being closer to the camera.

Our docking results show that in general short cationic linear peptides with amino acid length of 2-5 were not efficient in binding to HA. Pure anionic peptides can also be ruled out since HA is an anionic polymer which can cause charge-charge repulsion. This was also confirmed by the docking study of the anionic pentapeptide made up of aspartic acid (A5) which did not show any docked poses. Others have

found that anionic structures do not increase retention time in the VH.[18] Interestingly, Ax7A which is a linear octapeptide with two negatively charged aspartic acids and seven glycine amino acids (Table 3), exhibited good affinity toward HA and was comparable to the octapeptide Bx7B1 containing two positively charged arginine (Table 3). It is possible that the affinity is mainly due to the interactions with the peptide backbone, with only small contributions from the peptide side chains. To control for peptide backbone interaction with HA, addition of control peptides consisting of mono-glycine of varying lengths are needed.

The results indicate that increasing the linear peptide chain length, increased the strength of interaction, even up to 8-amino acid length. These docking studies also show that increasing the length of linear peptides from 8 to up to 25 residues led to a corresponding increase in their binding affinity toward HA. It should be noted that this study only considered linear peptides consisting of the polar, positively charged amino acid arginine in combination with the nonpolar amino acid glycine. Future studies should consider designing novel peptides containing other polar and non-polar amino acids.

We also investigated the effect of repeating units, up to 3 repeats (Bx7B1, Bx7B2, Bx7B3, Table 3). As expected, increasing the number of repeat units increased the affinity toward HA. This is likely due to the peptide having more sites to bind to HA. Future peptides should be constructed to look at Bx7B with longer glycine tails, to test the effect of polar and nonpolar contacts and its role in HA binding.

We also studied the effect of adding basic amino acids at the peptide terminals (BBx5BB and BBx6BB). It appears that these modifications led to greater binding with HA which suggests that peptides with additional nonpolar spacer glycine, exhibit better binding.

Peptides Bx7B1 and BBx6BB were selected due to their binding ability and length for further analysis. The top predicted binding poses for these peptides are shown in Figure 10.

The predicted binding of Bx7B1 shows that the basic guanidinium group at both ends of the peptide underwent electrostatic interaction with different carboxylic acid groups present in the structure of HA. Another electrostatic interaction in form of a salt-bridge was found between charged guanidino groups of

arginine and the carboxylic acid of HA. These electrostatic interactions anchor the peptide to the structure of HA. Interestingly, several intramolecular hydrogen bonding interactions formed at C-terminal of the designed peptide. In this way, the peptide bent back towards the N-terminal, maximizing the strength of electrostatic interactions between guanidinium side chain and carboxylic acid. The spacer region in the middle was stabilized by hydrogen bond interactions formed between the peptide backbone, glycine side chain and HA. The matrix of complex hydrogen bond interactions additively reinforces each other which can stabilize the peptide binding pose.

The predicted binding mode of BBx6BB with HA shows that the terminal arginine residues underwent electrostatic interactions with the carboxylic acid group in HA. The guanidinium group of arginine also underwent several hydrogen bonding interactions with D-glucuronic acid and N-acetyl-D-glucosamine units of HA.

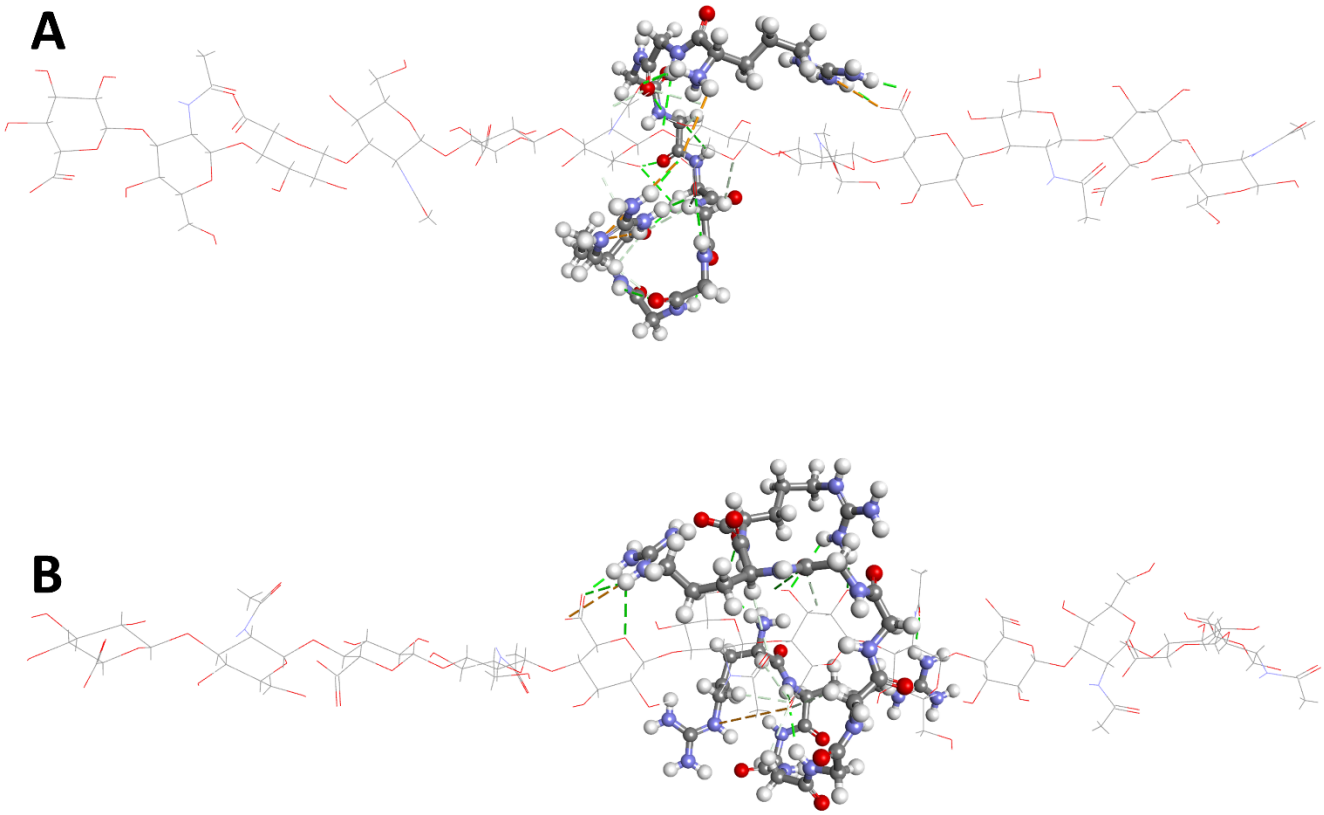


Figure 10. Predicted top ranking binding pose of candidate peptides (ball and stick cartoon) to 12-mer HA. The top ranking binding pose of (A) Bx7B1 and (B) BBx6BB are shown. Atoms of carbon, oxygen, nitrogen, and hydrogen (not displayed for HA) are displayed in grey, red, blue, and white, respectively. Intermolecular bonds between HA and peptides are displayed in green for hydrogen bond interactions and orange for electrostatic interactions. Lighter shaded interactions indicate the interaction being closer to the camera.

The limitations of this in silico study includes the fact that HA is not the sole molecular component found in the VH.[15,18] A better model to evaluate peptide affinity would include other macromolecular components of the VH such as collagens, which form mesh networks with HA, or the other glycosaminoglycans.[19] In addition, HA is a large molecular weight polymer consisting of several sugar units and its bound structure in the matrix is not known. Therefore, the present modeling study is a first step toward understanding the interactions of novel peptides with HA at the molecular level. It is clear that polar interactions such as electrostatic and hydrogen bonding interactions could be critical to design HA binding peptides. Furthermore, our drug delivery system uses exosomes conjugated with peptides, not peptides. It is possible that exosomal structure might prevent the binding of otherwise effective peptides.

### 3.5 Validating Exosome Conjugation

The sulfo-Cy3 azide conjugation protocol resulted in 0.46 ± 0.25% of the initial fluorophore being recovered in the pellet, compared to 0.05 ± 0.01 % in the control group (no exosomes); this difference was not statistically significant ($p > 0.05$). The protocol only resulted in 0.12 ± 0.04% of the initial exosomes being recovered in the pellet. Fluorescent NTA readings, on the other hand, indicated that of the exosomes recovered, 10.43 ± 4.38% of them could be detected by fluorescent NTA, showing moderate labeling efficiency. As expected, the control group (no exosomes) had no detectable signal under fluorescent NTA.

The control group with exosomes, sulfo-Cy3 azide, but no DBCO resulted in an exosome sample that could be detected using NTA under light mode, but not under fluorescent mode. This indicates that alkyne-functionalization of the exosomes was necessary for the azide-containing fluorophore to conjugate with the exosomes. The experimental group with sulfo-Cy3 azide, DBCO, but no exosomes resulted a sample that did not contain detectable particles (above solvent noise) under light or fluorescent mode. This group was evaluated because the azide-fluorophore and DBCO reagent are likely to form conjugation products. The results indicate that the UC protocol sufficiently washes these products such that they will not be mistaken for exosomes.

Similar values between exosome and fluorophore recovery likely suggest that poor fluorophore recovery is due to poor exosome recovery. In support of this conjecture, a significant fraction of recovered exosomes was fluorescent. Furthermore, it is likely that more than 10.43% of the exosomes were labeled, as this number is diminished by the limitations of fluorescent NTA. The peak emission of Cy3 is at 570 nm while the peak excitation is at 550 nm. Thus, as the laser module uses a fixed excitation wavelength at of 532 nm, the fluorophore was not maximally excited and thus also not maximally emitting fluorescence. This decreased the ability of the software to detect exosomes labeled with a smaller amount of Cy3. In fact, observation of the fluorescent NTA videos showed low intensity particle-like structures and movements that were likely weakly emitting exosomes (Figure 11A, 11C), but upon software analysis, many of these structures were not significant enough in duration or intensity to be considered in the

particle concentration analysis. On the other hand, light NTA frequently detected the exosomes at maximum intensity (Figure 11B, 11D). Potentially, the detection threshold or minimum trace length can be reduced while using fluorescent NTA to allow for inclusion of weakly emitting exosomes, as it is relatively unlikely for fluorescent NTA to have noise (compared to light NTA) due to a filter blocking non-fluorophore emissions. However, if the settings are differing between light and fluorescent NTA, it is not valid to compare the two groups to estimate the % of exosomes that are fluorescent. Thus, to optimize the accuracy of this estimation, it would be necessary evaluate and optimize machine settings that can detect most of the fluorescent exosomes while minimizing noise in light NTA. Photobleaching was not a concern because fluorescent NTA was performed with a syringe pump, which ensures flow of fresh non-photobleached particles to move into the flow cell to be detected.

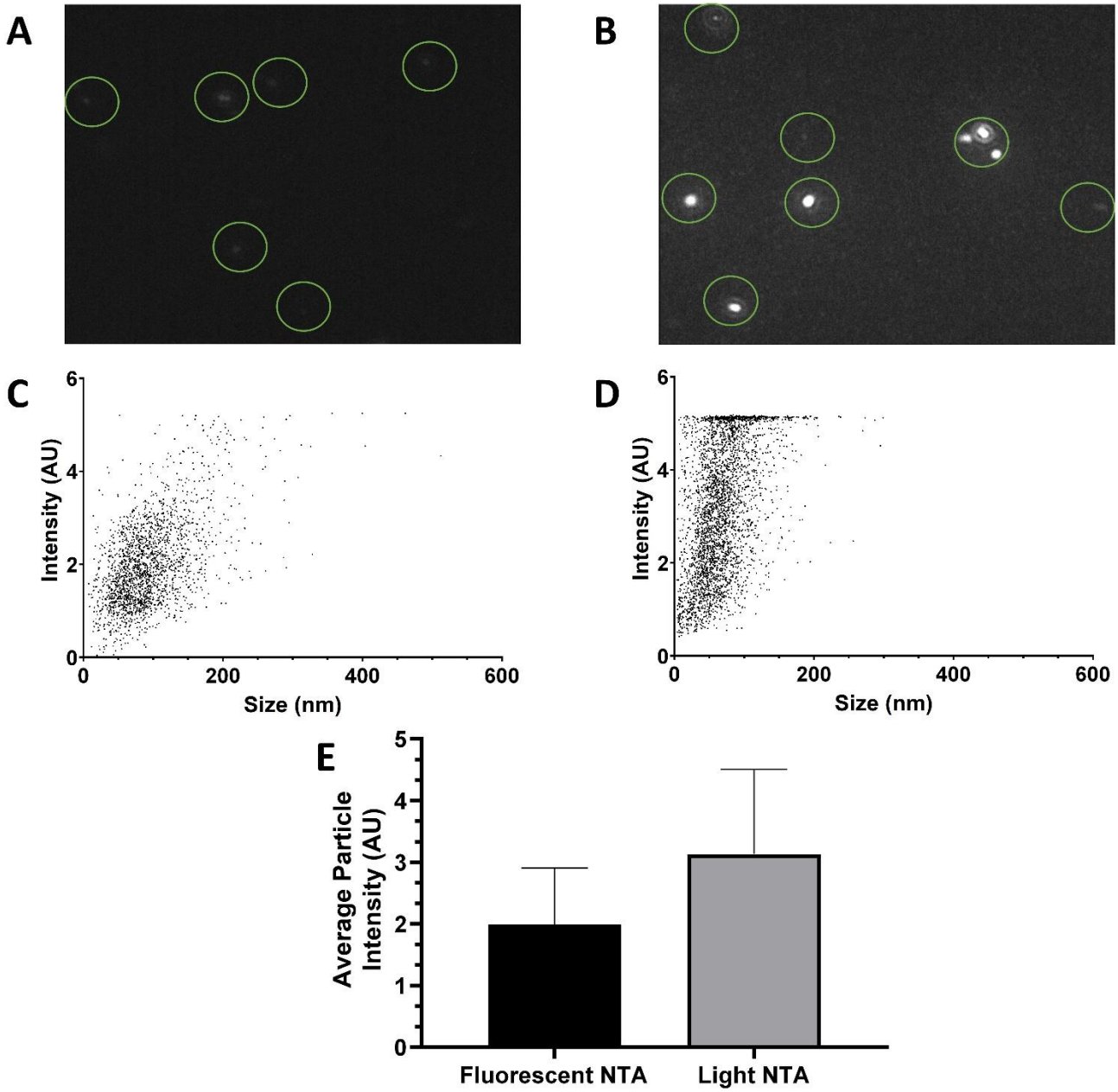


Figure 11. Representative NTA screen captures of cy3-labeled exosomes (A) using fluorescent-mode NTA (B) and light-mode NTA. Light and camera settings were identical. Green circles indicate areas where particles should be detected by the software. NTA size-intensity scatterplots of cy3-labeled exosomes as measured in (C) fluorescent-mode NTA (D) and light-mode NTA. Cy3-labeled exosomes often are detected at maximum intensity in light-mode NTA but not fluorescent-mode NTA. (E) Mean ± SD intensity of cy3-labeled exosome when measured in fluorescent-mode NTA (n = 2113) and light-mode NTA (n = 3440). The average intensity of a cy3-labeled exosome measured in light-mode NTA is significantly higher ($p<0.0001$) than when measured in fluorescent-mode NTA.

Nevertheless, there are potential adjustments that could be made to improve labeling efficiency. First, improving exosome recovery efficiency (by adjusting washing steps) will allow us to evaluate if

there are necessary improvements in fluorophore recovery. Second, reducing reaction volume or increasing reaction temperature of the functionalization step (DBCO with exosomes) and conjugation step (functionalized exosomes with azide-containing molecules) should improve efficiencies of both chemical processes. As volume decreases or temperature increases, interactions between molecules and particles becomes more frequent and thus it is more likely that the chemical-linkage will occur. Improvements in these steps would likely increase amounts of Cy3 being conjugated to the exosomes and manifest itself as improved labelling efficiency. Increasing reaction time beyond ~12 hours is unlikely to have a large effect, due to these reactions using NHS ester compounds, which hydrolyze rapidly in aqueous environments.

Thus, it was determined that the azide-alkyne chemistry was able to successfully form covalent links between exosomes and molecules of interest, and we could proceed with functionalization of exosomes with peptides. The limitations of this are that we did not actually validate the conjugation of the peptides to the exosomes, and thus it is possible that no peptides were actually conjugated to the exosomes. To confirm peptide conjugation efficiency, peptides should be radio-labeled or fluorescently labeled. However, fluorophores are large relative to the size of our peptides and thus might change its properties, thus radio-labeling is the better alternative to evaluate peptide conjugation efficiency.

## 3.6 Exosome Diffusion in HA Solution

### 3.6.1 Validity of the HA Diffusion Model

It was decided that a Franz-cell based model would be a suitable model to specifically evaluate how HA might affect the diffusion of exosomes with or without HA-binding peptides. In this design, the donor chamber was filled with HA solution, the receptor was filled with PBS, and the membrane should facilitate diffusion of exosomes but not HA. Under these conditions, addition of fluorescently labeled exosomes to the donor chamber should allow us to comparatively evaluate the effects of peptide conjugation, as interactions between HA-binding peptides and HA should in general, restrict diffusion within the donor chamber and thus also across the membrane.

As the first step of evaluating this model was to select a membrane that would prevent diffusion of HA across the membrane. As such, we needed a reliable way to measure the concentration of HA. Validation of this protocol was performed by evaluating a range of concentrations of HA (0 – 1000 µg/mL) and determining the range at which it displayed linearity. Linear regression indicated that the assay was linear between 0 – 250 µg/mL (Figure 12).

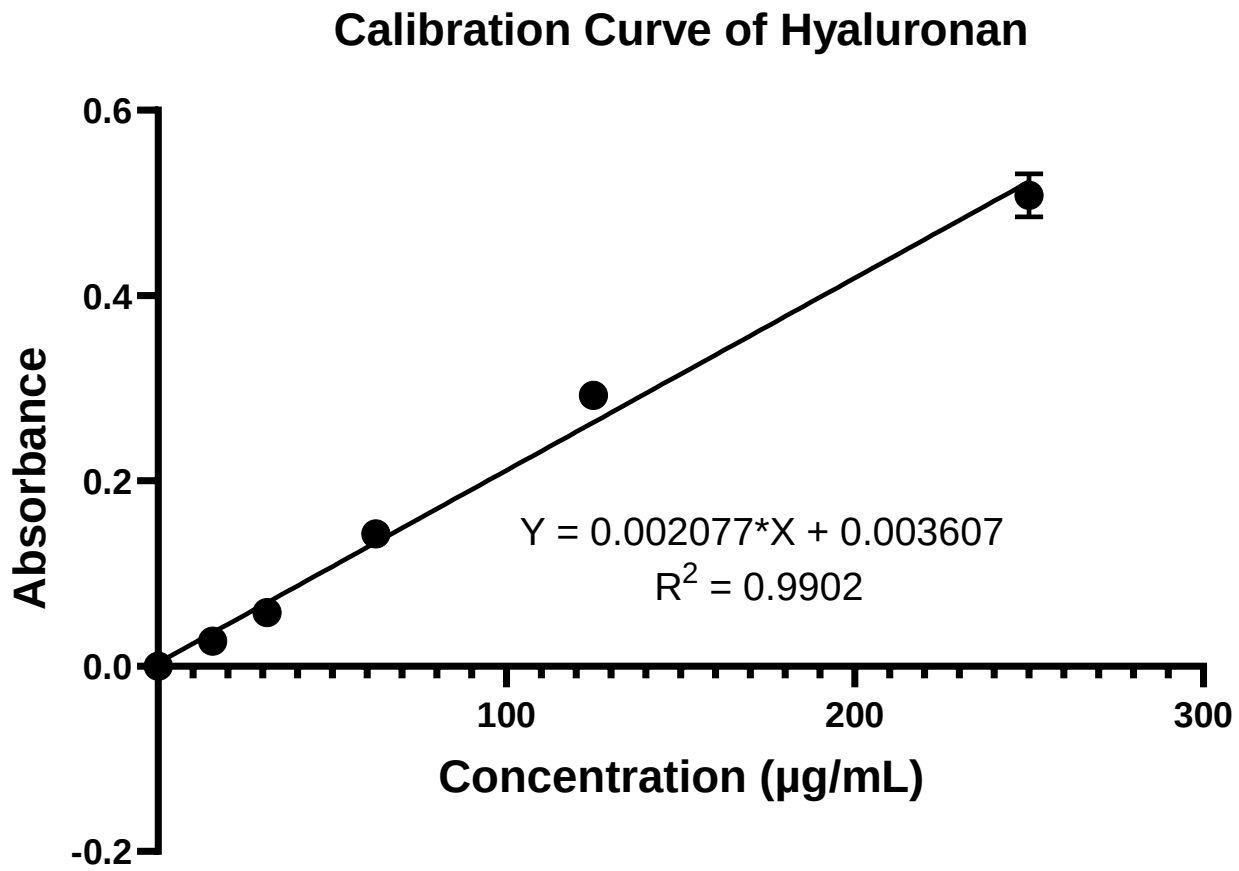


Figure 12. Calibration curve of HA. Known concentrations of HA (0 – 250 µg/mL) were used. Values at 500 and 1000 µg/mL were not included in the generation of the calibration curve. Absorbance was measured at 600 nm. Values represent mean ± SD (n = 3). Values were normalized by the blank average.

Our results indicate that the approximate hydrodynamic diameter of HA is between 0.1 and 0.2 µm and could be blocked by 0.1 µm pore size membrane filters (Figure 13). A naïve estimation of the hydrodynamic diameter of HA can be calculated based on an approximate equation describing the relationship between minimum diameter and Da for average spherical proteins:[120]

$$Diameter_{min} = 0.66M^{\frac{1}{3}}$$

*where M is molecular weight in Daltons*

Based on this equation, HA of 1.5 – 1.8 million Da should have approximate diameter of 76 – 80 nm and thus pass through 0.1 µm pore size membrane filters, at least in appreciable amounts. This estimation assumes an average protein density of 0.73 $cm^3/g$, spherical nature, and is a minimum value.[120] However, HA is a not spherical nor a globular protein, and thus using this estimation has limited validity.

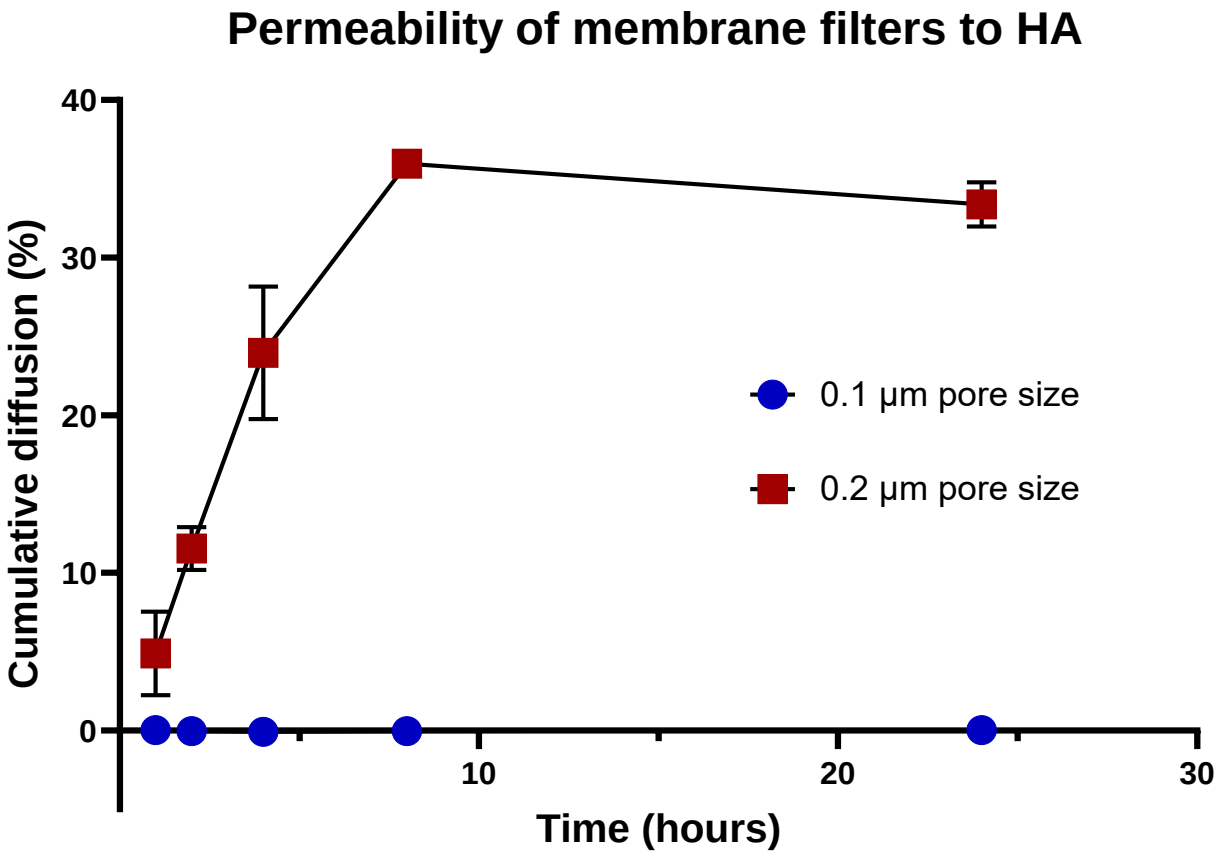


Figure 13. Permeability of membrane filters of different pore sizes (0.1 and 0.2 µm) to HA (MW 1.5-1.8 million Da) solution in PBS (1 mg/mL) in a diffusion cell, over various timepoints (1, 2, 4, 8, and 24 hrs). The temperature was set to 34°C. Measured concentrations were normalized to a cumulative percent of the initial concentration. Values represent mean ± SD (n = 3).

If HA was able to permeate the membranes, then there would be no way to accurately evaluate the hypothesis. Diffusion of exosome-HA complexes would pull exosomes through the membrane, which would be detected and remove any effect of the HA-binding peptides restricting diffusion.

There was concern that the 0.1 µm pore size membrane filter might block exosomes on the larger end of the size distribution (up to ~150 nm). As a result, we might observe a smaller effect size of peptide conjugation status than if an ideal pore size membrane filter were used, because the fraction of the exosome population above the pore size would not be diffusing through the membrane and thus not contributing to the effect size. However, it is important to note that pores sizes are stated as an average by manufacturers, and thus pores on the larger size of the distribution may facilitate diffusion of the larger exosomes, mitigating the effects noted above. Furthermore, purchasing and optimizing membrane filters pore size between 0.1 and 0.2 µm from manufacturers is simply not feasible. Instead, use of larger HA with greater molecular weight could potentially allow for the use of 0.2 µm pore size membrane filters. However, as there is no well-defined relationship between the molecular weight of HA and its hydrodynamic radius, this optimization experiment is beyond the scope of this thesis. Thus, we determined that our model had internal validity.

The external validity of this model is likely to have limitations. The model does not ideally mimic the biochemical, structural, or pharmacokinetic (fluid flow) aspects of the VH. For the biochemical limitations, our model lacks several components such as other glycosaminoglycans or collagens.[19] Both of these might alter binding of the peptides to HA. Human VH HA has molecular weights between 2 – 4 million Da,[18] which is significantly larger that the HA used in our model. HA is found in lower concentrations (0.1 – 0.4 mg/mL) in VH,[19] compared to the concentration used in the model (1 mg/mL). This might increase the retention of peptide-conjugate exosomes, as interactions between peptide and HA will be more likely at high HA concentrations.

The missing biochemical components also impart structure to the VH. Collagen and the glycosaminoglycans form mesh networks that create pores of various size.[15] These pores might significantly alter the diffusion of larger particles such as exosomes, while minimally affecting the diffusion of small molecules.[18] HA is found in highest concentrations near the retina,[19] and not in homogenous concentrations like our model. Since our model does not include collagen or

glycosaminoglycans, the diffusion kinetics observed may differ to a system that contains those components. In addition, we predict that diffusion rates will change as exosomes diffuses to areas with higher HA concentration. Viscosity is an additional parameter that can affect diffusion, but was not considered in this model. The viscosity of the VH is influenced by both the HA content and collagen content.[121] Altering our model to match the rheological characteristics of the VH might allow us to better evaluate the applicability of our system in the VH.

This model is different to other diffusion models in that the membrane is not the diffusion-limiting component. Instead, any particle that reaches the membrane should diffuse across the membrane without hinderance. In this model, diffusion within the HA solution in the donor chamber affects the amount of particles that can reach the membrane. If a particle's diffusion is restricted by its binding to HA, it will be less likely to reach the membrane through random diffusion. However, the gel-like nature of HA solution will also restrict fluid movement and thus also reduce diffusion, necessitating the right control groups to isolate the effect of peptide conjugation status.

### 3.6.2 Diffusion of Exosomes and Small Molecule Drugs in HA Solution

Both BBx6BB-functionalized exosomes and control exosomes could be detected in the receptor chamber after the 1 hour timepoint (Figure 14). Control exosomes were detected at significantly higher relative concentrations than peptide-functionalized exosomes at all timepoints. Only the dexamethasone-fluorescein group displayed diffusion and time-dependent increase in receptor concentration. Cumululative exosome concentrations appeared to decrease over time, which is potentially indicative of photobleaching or degradation of the fluorophores.

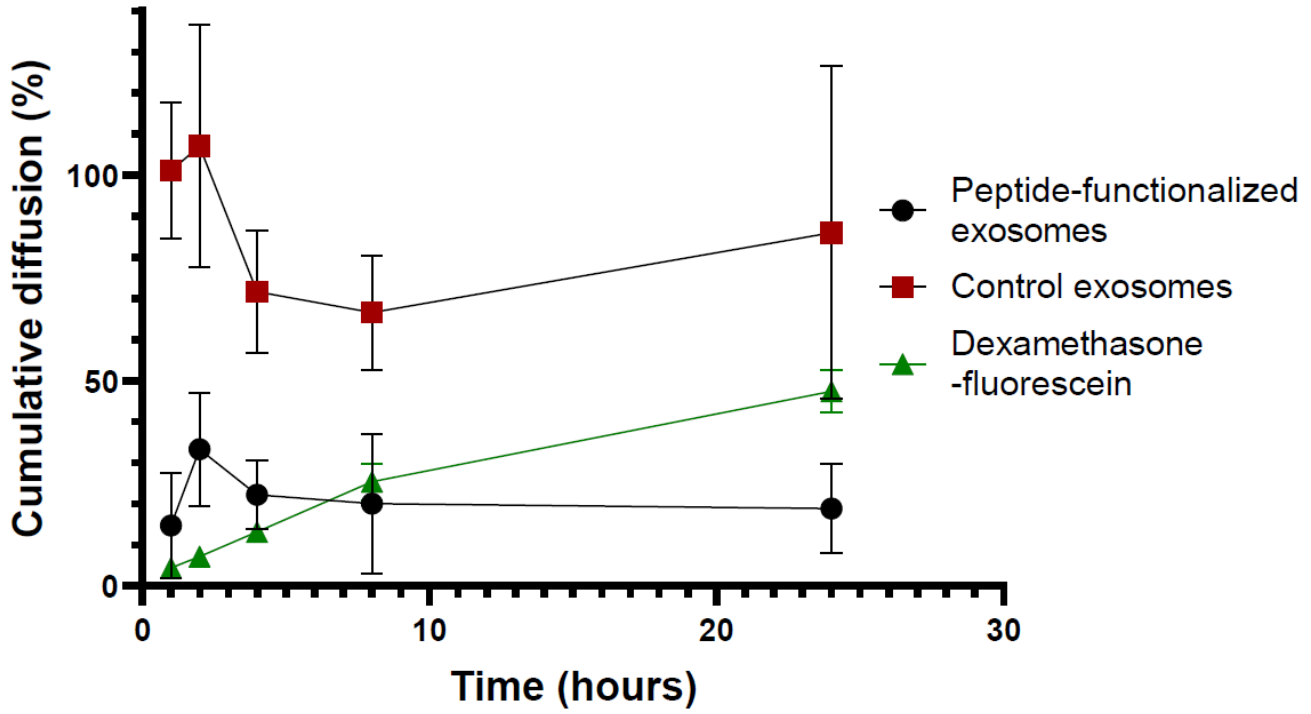


Figure 14. Diffusion of BBx6BB-functionalized exosomes and dexamethasone-fluorescein in the HA diffusion cell model over various timepoints (1, 2, 4, 8, and 24 hrs). Samples were mixed with HA solution in PBS (1 mg/mL) prior to addition to the donor chamber. The temperature was set to 34°C. The membrane filter used was 0.1 µm. Measured concentrations were normalized to a cumulative percent of the initial concentration. Values represent mean ± SD (n = 3).

As expected, dexamethasone-fluorescein exhibited consistent diffusion within the HA solution which allowed it to then diffuse across the membrane. Both exosomes groups showed high variance in diffusion over multiple timepoints. One explanantion for the large amount of variance seen in the exosome groups is low exosome fluorescence. With a lower initial fluorescence, the receptor fluorescence measurements clustered around the lower end (blank) of the calibration curve.

It is difficult to make a definitive conclusion on whether or not the peptides had an effect on the diffusion of the exosomes, for two reasons. First, the mean of first data point for the control exosome group suggests maximal diffusion has occurred at the 1 hr timepoint. However, it is unlikely that unmodified exosomes are diffusing across the membrane faster than dexamethasone-fluorescein. Second, due to the high variance of data points for both exosome groups, it is difficult to tell if diffusion is occuring or not, and in which direction.

These challenges would be best solved by significantly increasing the amount of concentration of the initial fluorescently-labeled exosomes. By increasing the initial amount of fluorescence, the the receptor fluorescence measurements should be higher and thus less clustered around the lower end of the calibration curve. By increasing the initial amount of exosomes, variance in diffusion should be reduced as a larger population of exosomes are being observed. Sampling of additional timepoints between 0 and 1 hour will allow us to better evaluate the burst diffusion seemingly observed with the exosome groups.

# Chapter 4: Conclusions and Future Directions

Pharmacological treatment of retinal diseases such as DR is limited by poor pharmacokinetics or drug properties, which renders many pharmacotherapies unfeasible due to effectiveness or compliance.[18,26,31] In order to develop drug delivery systems that can bypass these limitations, novel strategies need to be applied. As diffusion is one of the primary means of drug clearance from the VH, developing drug delivery systems that have restricted diffusion is a promising strategy.[26,31] Of these strategies, modulation of the system with cationic properties or HA-binding modules to confer HA-binding has been investigated.[15,34,35] Use of nanotechnology can also improve effectiveness of pharmacotherapies by providing protection against degradation, allow for use of supratherapeutic doses (by controlling release), and in this case, acting as carrier that can be modified to suit the intended application.

Here, we describe the design of specific HA-binding peptides for conjugation to exosomes, along with the characterization of these exosomes in an in-vitro model that can be used to make preliminary evaluations on the effectiveness of HA-binding drug delivery systems. Further experimentation and optimization of the peptide-functionalized exosome drug delivery system, along with evaluation in increasingly ecologically valid models, is necessary. In general, optimization of the methods used to work with exosomes is necessary for further development of exosome-based drug delivery systems.[103] Cell uptake of exosomes should be quantitated in a variety of relevant cell lines, including but not limited to

Müller cells or vascular endothelial cells. Although drug-loading and release has been previously achieved with exosomes of other sources, it is necessary to show that ARPE19 isolated exosomes also have these properties. Cell viability assays should be conducted to ensure that exosomes or any modified exosomes are safe. Following this, safety can be evaluated in animal toxicity studies. Improvements and progression with the model should be made as well, such as using liquified VH in place of HA solution. Use of excised VH along with confocal microscopy for single-particle tracking has shown to be a relevant and simple model to evaluate particle diffusion in the VH.[15] Optimal peptide design can be investigated further using molecular docking followed by testing in the relevant models. Finally, in-vivo pharmacokinetic and efficacy studies can be done as the culmination of all the addition studies and optimizations.

Use of exosomes for drug delivery to the eye in general, is a novel area. There are numerous potential applications for use of exosomes for drug delivery, including to ocular surface diseases such as dry eye disease, corneal abrasion, bacterial conjunctivitis, and many others. Due to the infancy of exosome drug delivery in these areas, it will be necessary to diligently evaluate the specific details of the disease, anatomy, physiology, and pharmacology, to intelligently design a safe and effective drug delivery system. Our work has demonstrated several techniques and shown some of the challenges of working with exosome-based drug delivery systems and can serve as a platform on which to build other exosome-based drug delivery systems for treatment of ocular diseases.

# References


1. Ruta, L. M. *et al.* Prevalence of diabetic retinopathy in Type 2 diabetes in developing and developed countries. *Diabet Med* **30**, 387–398 (2013).

2. Solomon, S. D. *et al.* Diabetic Retinopathy: A Position Statement by the American Diabetes Association. *Diabetes Care* **40**, 412–418 (2017).

3. Hendrick, A. M., Gibson, M. V. & Kulshreshtha, A. Diabetic Retinopathy. *Prim Care* **42**, 451–464 (2015).

4. Kuroki, M. *et al.* Reactive oxygen intermediates increase vascular endothelial growth factor expression in vitro and in vivo. *J Clin Invest* **98**, 1667–1675 (1996).

5. Ablonczy, Z. & Crosson, C. E. VEGF Modulation of Retinal Pigment Epithelium Resistance. *Exp Eye Res* **85**, 762–771 (2007).

6. Tarr, J. M., Kaul, K., Chopra, M., Kohner, E. M. & Chibber, R. Pathophysiology of Diabetic Retinopathy. *ISRN Ophthalmol* **2013**, (2013).

7. Salz, D. A. & Witkin, A. J. Imaging in Diabetic Retinopathy. *Middle East Afr J Ophthalmol* **22**, 145–150 (2015).

8. Duh, E. J., Sun, J. K. & Stitt, A. W. Diabetic retinopathy: current understanding, mechanisms, and treatment strategies. *JCI Insight* **2**,.

9. Preliminary report on effects of photocoagulation therapy. The Diabetic Retinopathy Study Research Group. *Am J Ophthalmol* **81**, 383–396 (1976).

10. Photocoagulation for diabetic macular edema. Early Treatment Diabetic Retinopathy Study report number 1. Early Treatment Diabetic Retinopathy Study research group. *Arch Ophthalmol* **103**, 1796–1806 (1985).

11. Cheung, N., Wong, I. Y. & Wong, T. Y. Ocular Anti-VEGF Therapy for Diabetic Retinopathy: Overview of Clinical Efficacy and Evolving Applications. *Diabetes Care* **37**, 900–905 (2014).

12. Lattanzio, R., Cicinelli, M. V. & Bandello, F. Intravitreal Steroids in Diabetic Macular Edema. *Dev Ophthalmol* **60**, 78–90 (2017).

13. Zhang, X., Wang, N., Schachat, A. P., Bao, S. & Gillies, M. C. Glucocorticoids: Structure, Signaling and Molecular Mechanisms in the Treatment of Diabetic Retinopathy and Diabetic Macular Edema. *Curr Mol Med* **14**, 376–384 (2014).

14. Ansari, M. W. & Nadeem, A. *Atlas of Ocular Anatomy*. (Springer International Publishing, 2016).

15. Xu, Q. *et al.* Nanoparticle diffusion in, and microrheology of, the bovine vitreous ex vivo. *J. Control Release* **167**, 76–84 (2013).

16. Theocharis, D. A., Feretis, E. & Papageorgacopoulou, N. Glycosaminoglycans in the vitreous body of patients with retinal detachment. *Biochem Int* **25**, 397–407 (1991).

17. Rapport, M. M., Weissmann, B., Linker, A. & Meyer, K. Isolation of a Crystalline Disaccharide, Hyalobiuronic Acid, from Hyaluronic Acid. *Nature* **168**, 996–997 (1951).

18. del Amo, E. M. *et al.* Pharmacokinetic aspects of retinal drug delivery. *Prog Retin Eye Res* **57**, 134–185 (2017).

19. Balazs, E. A. Physiology of the vitreous body. *Importance Vitr Body Retina Surg Spec Emphas Reoperations* 29–48 (1960).

20. Wong-Riley, M. Energy metabolism of the visual system. *Eye Brain* **2**, 99–116 (2010).

21. Pitkänen, L., Ranta, V.-P., Moilanen, H. & Urtti, A. Permeability of Retinal Pigment Epithelium: Effects of Permeant Molecular Weight and Lipophilicity. *Invest Ophthalmol Vis Sci* **46**, 641–646 (2005).

22. Kay, P., Yang, Y. C. & Paraoan, L. Directional protein secretion by the retinal pigment epithelium: roles in retinal health and the development of age-related macular degeneration. *J Cell Mol Med* **17**, 833–843 (2013).

23. Xu, H.-Z., Song, Z., Fu, S., Zhu, M. & Le, Y.-Z. RPE barrier breakdown in diabetic retinopathy: seeing is believing. *J Ocul Biol Dis Infor* **4**, 83–92 (2011).

24. Gaudana, R., Ananthula, H. K., Parenky, A. & Mitra, A. K. Ocular Drug Delivery. *AAPS J* **12**, 348–360 (2010).

25. McLaren, J. W. Measurement of aqueous humor flow. *Exp Eye Res* **88**, 641–647 (2009).

26. del Amo, E. M., Vellonen, K.-S., Kidron, H. & Urtti, A. Intravitreal clearance and volume of distribution of compounds in rabbits: In silico prediction and pharmacokinetic simulations for drug development. *Eur J Pharm Biopharm* **95**, 215–226 (2015).

27. Duvvuri, S., Majumdar, S. & Mitra, A. K. Role of Metabolism in Ocular Drug Delivery. *Curr Drug Metab* **5**, 507–515 (2004).

28. Ghasemi Falavarjani, K. & Nguyen, Q. D. Adverse events and complications associated with intravitreal injection of anti-VEGF agents: a review of literature. *Eye* **27**, 787–794 (2013).

29. Polat, O. *et al.* Factors Affecting Compliance to Intravitreal Anti-Vascular Endothelial Growth Factor Therapy in Patients with Age-Related Macular Degeneration. *Turk J Ophthalmol* **47**, 205–210 (2017).

30. Cohen, S. Y. *et al.* Changes In Visual Acuity In Patients With Wet Age-related Macular Degeneration Treated With Intravitreal Ranibizumab In Daily Clinical Practice: The Lumiere Study. *Retina* **33**, 474–481 (2013).

31. Shatz, W., Aaronson, J., Yohe, S., Kelley, R. F. & Kalia, Y. N. Strategies for modifying drug residence time and ocular bioavailability to decrease treatment frequency for back of the eye diseases. *Expert Opin Drug Deliv* **16**, 43–57 (2019).

32. Rodrigues, G. A. *et al.* Functional Characterization of Abicipar-Pegol, an Anti-VEGF DARPin Therapeutic That Potently Inhibits Angiogenesis and Vascular Permeability. *Invest Ophthalmol Vis Sci* **59**, 5836–5846 (2018).

33. Hughes, S. *et al.* Prolonged intraocular residence and retinal tissue distribution of a fourth-generation compstatin-based C3 inhibitor in non-human primates. *Clin Immunol* **214**, 108391 (2020).

34. Ghosh, J. G. *et al.* Long-acting protein drugs for the treatment of ocular diseases. *Nat Commun.* **8**, 14837 (2017).

35. Melgar-Asensio, I. *et al.* Extended Intravitreal Rabbit Eye Residence of Nanoparticles Conjugated With Cationic Arginine Peptides for Intraocular Drug Delivery: In Vivo Imaging. *Invest Ophthalmol Vis Sci* **59**, 4071–4081 (2018).

36. Day, A. J. & Prestwich, G. D. Hyaluronan-binding Proteins: Tying Up the Giant. *J Biol Chem* **277**, 4585–4588 (2002).

37. Amemiya, K., Nakatani, T., Saito, A., Suzuki, A. & Munakata, H. Hyaluronan-binding motif identified by panning a random peptide display library. *Biochim Biophys Acta* **1724**, 94–99 (2005).

38. Yang, B., Yang, B. L., Savani, R. C. & Turley, E. A. Identification of a common hyaluronan binding motif in the hyaluronan binding proteins RHAMM, CD44 and link protein. *EMBO J* **13**, 286–296 (1994).

39. Kohda, D. *et al.* Solution structure of the link module: a hyaluronan-binding domain involved in extracellular matrix stability and cell migration. *Cell* **86**, 767–775 (1996).

40. The tandemly repeated sequences of cartilage link protein contain the sites for interaction with hyaluronic acid. *J Cell Biol* **105**, 2403–2408 (1987).

41. Sliwoski, G., Kothiwale, S., Meiler, J. & Lowe, E. W. Computational Methods in Drug Discovery. *Pharmacol Rev* **66**, 334–395 (2014).

42. Pagadala, N. S., Syed, K. & Tuszynski, J. Software for molecular docking: a review. *Biophys Rev* **9**, 91–102 (2017).

43. Sulimov, V. B., Kutov, D. C. & Sulimov, A. V. Advances in Docking. *Curr Med Chem* **26**, 7555–7580 (2019).

44. Berman, H. M. *et al.* The Protein Data Bank. *Nucleic Acids Res* **28**, 235–242 (2000).

45. Kalra, H. *et al.* Vesiclepedia: A Compendium for Extracellular Vesicles with Continuous Community Annotation. *PLoS Biol* **10**, (2012).

46. Hessvik, N. P. & Llorente, A. Current knowledge on exosome biogenesis and release. *Cell Mol Life Sci* **75**, 193–208 (2018).

47. Pan, B.-T. & Johnstone, R. M. Fate of the transferrin receptor during maturation of sheep reticulocytes in vitro: Selective externalization of the receptor. *Cell* **33**, 967–978 (1983).

48. Mathivanan, S., Ji, H. & Simpson, R. J. Exosomes: Extracellular organelles important in intercellular communication. *J Proteomics* **73**, 1907–1920 (2010).

49. Schwendener, R. A. & Schott, H. Liposome Formulations of Hydrophobic Drugs. *Methods Mol Biol* **605**, 129–138 (2010).

50. Sun, D. *et al.* A Novel Nanoparticle Drug Delivery System: The Anti-inflammatory Activity of Curcumin Is Enhanced When Encapsulated in Exosomes. *Mol Ther* **18**, 1606–1614 (2010).

51. Kim, M. *et al.* Development of exosome-encapsulated paclitaxel to overcome MDR in cancer cells. *Nanomedicine* **12**, 655–664 (2016).

52. Yang, T. *et al.* Exosome Delivered Anticancer Drugs Across the Blood-Brain Barrier for Brain Cancer Therapy in Danio Rerio. *Pharm Res* **32**, 2003–2014 (2015).

53. Tian, T. *et al.* Surface functionalized exosomes as targeted drug delivery vehicles for cerebral ischemia therapy. *Biomaterials* **150**, 137–149 (2018).

54. Alvarez-Erviti, L. *et al.* Delivery of siRNA to the mouse brain by systemic injection of targeted exosomes. *Nat Biotechnol* **29**, 341–345 (2011).

55. Hajrasouliha, A. *et al.* Exosomes from Retinal Astrocytes Contain Antiangiogenic Components That Inhibit Laser-induced Choroidal Neovascularization. *J Biol Chem* **288**, 28058–28067 (2013).

56. Dunn, K. C., Aotaki-keen, A. E., Putkey, F. R. & Hjelmeland, L. M. ARPE-19, A Human Retinal Pigment Epithelial Cell Line with Differentiated Properties. *Exp Eye Res* **62**, 155–170 (1996).

57. Sandra, A.-A. *et al.* Oxidative stress in retinal pigment epithelium cells increases exosome secretion and promotes angiogenesis in endothelial cells. *J Cell Mol Med* **20**, 1457–1466 (2016).

58. Théry, C. *et al.* Minimal information for studies of extracellular vesicles 2018 (MISEV2018): a position statement of the International Society for Extracellular Vesicles and update of the MISEV2014 guidelines. *J Extracell Vesicles* **7**, 1535750 (2018).

59. Patel, D. B. *et al.* Impact of cell culture parameters on production and vascularization bioactivity of mesenchymal stem cell-derived extracellular vesicles. *Bioeng Transl Med* **2**, 170–179 (2017).

60. Gudbergsson, J. M., Johnsen, K. B., Skov, M. N. & Duroux, M. Systematic review of factors influencing extracellular vesicle yield from cell cultures. *Cytotechnology* **68**, 579–592 (2016).

61. Kornilov, R. *et al.* Efficient ultrafiltration-based protocol to deplete extracellular vesicles from fetal bovine serum. *J Extracell Vesicles* **7**, 1422674 (2018).

62. Yan, I. K., Shukla, N., Borrelli, D. A. & Patel, T. Use of a Hollow Fiber Bioreactor to Collect Extracellular Vesicles from Cells in Culture. *Methods Mol Biol* **1740**, 35–41 (2018).

63. Sabnis, N. & Lacko, A. G. Drug delivery via lipoprotein-based carriers: answering the challenges in systemic therapeutics. *Ther Deliv* **3**, 599–608 (2012).

64. Yuana, Y., Levels, J., Grootemaat, A., Sturk, A. & Nieuwland, R. Co-isolation of extracellular vesicles and high-density lipoproteins using density gradient ultracentrifugation. *J Extracell Vesicles* **3**, 23262 (2014).

65. Grigor'eva, A. E. *et al.* Contamination of exosome preparations, isolated from biological fluids. *Biomed Khim* **63**, 91–96 (2017).

66. Cvjetkovic, A., Lötvall, J. & Lässer, C. The influence of rotor type and centrifugation time on the yield and purity of extracellular vesicles. *J Extracell Vesicles* **3**, (2014).

67. Lobb, R. J. *et al.* Optimized exosome isolation protocol for cell culture supernatant and human plasma. *J Extracell Vesicles* **4**, 27031 (2015).

68. Sódar, B. W. *et al.* Low-density lipoprotein mimics blood plasma-derived exosomes and microvesicles during isolation and detection. *Sci Rep* **6**, 24316 (2016).

69. Onódi, Z. *et al.* Isolation of High-Purity Extracellular Vesicles by the Combination of Iodixanol Density Gradient Ultracentrifugation and Bind-Elute Chromatography From Blood Plasma. *Front Physiol* **9**, (2018).

70. Baranyai, T. *et al.* Isolation of Exosomes from Blood Plasma: Qualitative and Quantitative Comparison of Ultracentrifugation and Size Exclusion Chromatography Methods. *PLoS One* **10**, e0145686 (2015).

71. Ana, G.-V. *et al.* Size-Exclusion Chromatography-based isolation minimally alters Extracellular Vesicles' characteristics compared to precipitating agents. *Sci Rep* **6**, srep33641 (2016).

72. Böing, A. *et al.* Single-step isolation of extracellular vesicles by size-exclusion chromatography. *J Extracell Vesicles* **3**, (2014).

73. Hagel, L., Östberg, M. & Andersson, T. Apparent pore size distributions of chromatography media. *J Chromatogr A* **743**, 33–42 (1996).

74. Burgess, R. R. A brief practical review of size exclusion chromatography: Rules of thumb, limitations, and troubleshooting. *Protein Expr Purif* **150**, 81–85 (2018).

75. Heinemann, M. L. *et al.* Benchtop isolation and characterization of functional exosomes by sequential filtration. *J Chromatogr A* **1371**, 125–135 (2014).

76. Busatto, S. *et al.* Tangential Flow Filtration for Highly Efficient Concentration of Extracellular Vesicles from Large Volumes of Fluid. *Cells* **7**, 273 (2018).

77. Zarovni, N. *et al.* Integrated isolation and quantitative analysis of exosome shuttled proteins and nucleic acids using immunocapture approaches. *Methods* **87**, 46–58 (2015).

78. Patel, G. K. *et al.* Comparative analysis of exosome isolation methods using culture supernatant for optimum yield, purity and downstream applications. *Sci Rep* **9**, 5335 (2019).

79. Palanisamy, V. *et al.* Nanostructural and Transcriptomic Analyses of Human Saliva Derived Exosomes. *PLoS One* **5**, e8577 (2010).

80. Tian, T., Wang, Y., Wang, H., Zhu, Z. & Xiao, Z. Visualizing of the cellular uptake and intracellular trafficking of exosomes by live-cell microscopy. *J Cell Biochem* **111**, 488–496 (2010).

81. Sharma, S. *et al.* Structural-Mechanical Characterization of Nanoparticle Exosomes in Human Saliva, Using Correlative AFM, FESEM, and Force Spectroscopy. *ACS Nano* **4**, 1921–1926 (2010).

82. Paolini, L. *et al.* Residual matrix from different separation techniques impacts exosome biological activity. *Sci Rep* **6**, 23550 (2016).

83. Whitehead, B. *et al.* Tumour exosomes display differential mechanical and complement activation properties dependent on malignant state: implications in endothelial leakiness. *J Extracell Vesicles* **4**, 29685 (2015).

84. Sebaihi, N., Boeck, B. D., Yuana, Y., Nieuwland, R. & Pétry, J. Dimensional characterization of extracellular vesicles using atomic force microscopy. *Meas Sci Technol* **28**, 034006 (2017).

85. Calò, A. *et al.* Force measurements on natural membrane nanovesicles reveal a composition-independent, high Young's modulus. *Nanoscale* **6**, 2275–2285 (2014).

86. Rikkert, L. G., Nieuwland, R., Terstappen, L. W. M. M. & Coumans, F. A. W. Quality of extracellular vesicle images by transmission electron microscopy is operator and protocol dependent. *J Extracell Vesicles* **8**, (2019).

87. Pisitkun, T., Shen, R.-F. & Knepper, M. A. Identification and proteomic profiling of exosomes in human urine. *Proc Natl Acad Sci* **101**, 13368–13373 (2004).

88. Sokolova, V. *et al.* Characterisation of exosomes derived from human cells by nanoparticle tracking analysis and scanning electron microscopy. *Colloids Surf B Biointerfaces* **87**, 146–150 (2011).

89. Pol, E. V. D. *et al.* Optical and non-optical methods for detection and characterization of microparticles and exosomes. *J Thromb Haemost* **8**, 2596–2607 (2010).

90. Pol, E. van der *et al.* Particle size distribution of exosomes and microvesicles determined by transmission electron microscopy, flow cytometry, nanoparticle tracking analysis, and resistive pulse sensing. *J Thromb Haemost* **12**, 1182–1192 (2014).

91. van der Vlist, E. J., Nolte-'t Hoen, E. N. M., Stoorvogel, W., Arkesteijn, G. J. A. & Wauben, M. H. M. Fluorescent labeling of nano-sized vesicles released by cells and subsequent quantitative and qualitative analysis by high-resolution flow cytometry. *Nat Protoc* **7**, 1311–1326 (2012).

92. Pospichalova, V. *et al.* Simplified protocol for flow cytometry analysis of fluorescently labeled exosomes and microvesicles using dedicated flow cytometer. *J Extracell Vesicles* **4**, 25530 (2015).

93. McVey, M. J., Spring, C. M. & Kuebler, W. M. Improved resolution in extracellular vesicle populations using 405 instead of 488 nm side scatter. *J Extracell Vesicles* **7**, 1454776 (2018).

94. Thane, K. E., Davis, A. M. & Hoffman, A. M. Improved methods for fluorescent labeling and detection of single extracellular vesicles using nanoparticle tracking analysis. *Sci Rep* **9**, 12295 (2019).

95. Dragovic, R. A. *et al.* Sizing and phenotyping of cellular vesicles using Nanoparticle Tracking Analysis. *Nanomedicine* **7**, 780–788 (2011).

96. Vestad, B. *et al.* Size and concentration analyses of extracellular vesicles by nanoparticle tracking analysis: a variation study. *J Extracell Vesicles* **6**, 1344087 (2017).

97. Anderson, W., Lane, R., Korbie, D. & Trau, M. Observations of Tunable Resistive Pulse Sensing for Exosome Analysis: Improving System Sensitivity and Stability. *Langmuir* **31**, 6577–6587 (2015).

98. Maroto, R. *et al.* Effects of storage temperature on airway exosome integrity for diagnostic and functional analyses. *J Extracell Vesicles* **6**, 1359478 (2017).

99. Lőrincz, Á. M. *et al.* Effect of storage on physical and functional properties of extracellular vesicles derived from neutrophilic granulocytes. *J Extracell Vesicles* **3**, 25465 (2014).

100. Charoenviriyakul, C., Takahashi, Y., Nishikawa, M. & Takakura, Y. Preservation of exosomes at room temperature using lyophilization. *Int J Pharm* **553**, 1–7 (2018).

101. Bosch, S. *et al.* Trehalose prevents aggregation of exosomes and cryodamage. *Sci Rep* **6**, 36162 (2016).

102. Cheng, Y., Zeng, Q., Han, Q. & Xia, W. Effect of pH, temperature and freezing-thawing on quantity changes and cellular uptake of exosomes. *Protein Cell* **10**, 295–299 (2019).

103. Wang, J., Chen, D. & Ho, E. A. Challenges in the development and establishment of exosome-based drug delivery systems. *J Control Release* **329**, 894–906 (2020).

104. Richardson, J. J. & Ejima, H. Surface Engineering of Extracellular Vesicles through Chemical and Biological Strategies. *Chem Mater* **31**, 2191–2201 (2019).

105. Hein, C. D., Liu, X.-M. & Wang, D. Click Chemistry, a Powerful Tool for Pharmaceutical Sciences. *Pharm Res* **25**, 2216–2230 (2008).

106. Smyth, T. *et al.* Surface Functionalization of Exosomes Using Click Chemistry. *Bioconjug Chem* **25**, 1777–1784 (2014).

107. Wu, G., Robertson, D. H., Brooks, C. L. & Vieth, M. Detailed analysis of grid-based molecular docking: A case study of CDOCKER-A CHARMm-based MD docking algorithm. *J Comput Chem* **24**, 1549–1562 (2003).

108. Rao, P. P. N., Mohamed, T., Teckwani, K. & Tin, G. Curcumin Binding to Beta Amyloid: A Computational Study. *Chem Biol Drug Des* **86**, 813–820 (2015).

109. Ferrante, N. D. Turbidimetric Measurement of Acid Mucopoly-Saccharides and Hyaluronidase Activity. *J Biol Chem* **220**, 303–306 (1956).

110. Nakai, W. *et al.* A novel affinity-based method for the isolation of highly purified extracellular vesicles. *Sci Rep* **6**, 1–11 (2016).

111. Skipski, V. P. *et al.* Lipid composition of human serum lipoproteins. *Biochem J* **104**, 340352 (1967).

112. Dunn, K. C., Aotaki-keen, A. E., Putkey, F. R. & Hjelmeland, L. M. ARPE-19, A Human Retinal Pigment Epithelial Cell Line with Differentiated Properties. *Exp Eye Res* **62**, 155–170 (1996).

113. Kapuscinski, J. DAPI: a DNA-Specific Fluorescent Probe. *Biotech Histochem* **70**, 220–233 (1995).

114. Chazotte, B. Labeling Nuclear DNA Using DAPI. *Cold Spring Harb Protoc* **2011**, pdb.prot5556 (2011).

115. Horibe, S., Tanahashi, T., Kawauchi, S., Murakami, Y. & Rikitake, Y. Mechanism of recipient cell-dependent differences in exosome uptake. *BMC Cancer* **18**, 47 (2018).

116. McKelvey, K. J., Powell, K. L., Ashton, A. W., Morris, J. M. & McCracken, S. A. Exosomes: Mechanisms of Uptake. *J Circ Biomark* **4**, 7 (2015).

117. Barber, A. J. A new view of diabetic retinopathy: a neurodegenerative disease of the eye. *Prog. Neuropsychopharmacol Biol Psychiatry* **27**, 283–290 (2003).

118. Weinreb, R. N., Polansky, J. R., Kramer, S. G. & Baxter, J. D. Acute effects of dexamethasone on intraocular pressure in glaucoma. *Invest Ophthalmol Vis Sci* **26**, 170–175 (1985).

119. Iglicki, M., Zur, D., Busch, C., Okada, M. & Loewenstein, A. Progression of diabetic retinopathy severity after treatment with dexamethasone implant: a 24-month cohort study the 'DR-Pro-DEX Study'. *Acta Diabetol* **55**, 541–547 (2018).

120. Erickson, H. P. Size and Shape of Protein Molecules at the Nanometer Level Determined by Sedimentation, Gel Filtration, and Electron Microscopy. *Biol Proced. Online* **11**, 32–51 (2009).

121. Silva, A. F., Alves, M. A. & Oliveira, M. S. N. Rheological behaviour of vitreous humour. *Rheol Acta* **56**, 377–386 (2017).